The effect of overshooting 1.5°C global warming on the mass loss of the Greenland Ice Sheet

Martin Rückamp[1], Ulrike Falk[2], Katja Frieler[3], Stefan Lange[3], and Angelika Humbert[1,4]

[1]Alfred Wegener Institute, Helmholtz Centre for Polar and Marine Research, Bremerhaven, Germany
[2]formerly Alfred Wegener Institute, Helmholtz Centre for Polar and Marine Research, Bremerhaven, Germany
[3]Potsdam Institute for Climate Impact Research, Potsdam, Germany
[4]University of Bremen, Bremen, Germany

Correspondence to: martin.rueckamp@awi.de

Abstract. Sea level rise associated with changing climate is expected to pose a major challenge for societies. Based on the efforts of COP21 to limit global warming to 2.0°C or even 1.5°C by the end of 21^{th} century (Paris Agreement), we simulate the future contribution of the Greenland ice sheet (GrIS) to sea level change under the low emission representative concentration pathway (RCP) 2.6 scenario. The ice sheet model ISSM with higher order approximation is used and initialized with a hybrid approach between spin-up and data assimilation. For three general circulation models (HadGEM2-ES, IPSL-CM5A-LR, MIROC5) the projections are conducted up to 2300 with forcing fields for surface mass balance (SMB) and ice surface temperature (T_s) computed by the SEMIC model (Krapp et al., 2017). The projected sea level rise ranges between 21–38 mm by 2100 and 36–85 mm by 2300. According to the three GCMs used, warming of 1.5°C has been exceeded early in the 21^{th} century. The RCP2.6 peak and decline scenario is therefore in a another set of experiments manually adjusted to suppress the 1.5°C-overshooting effect. These scenarios show a sea level contribution that is on average about 38% and 31% less by 2100 and 2300, respectively. The rate of mass loss in 23^{rd} century is for some scenarios not excluding a stable ice sheet. This is most likely due to an integrated SMB that never fall below zero, or even a recovery of SMB towards values of slightly below present day. Although the mean SMB is reduced in the warmer climate, a future steady-state ice sheet with lower surface elevation and hence volume might be possible. Our results indicate, that uncertainties stem from the underlying climate model to calculate the surface mass balance. However, the RCP2.6 scenario will lead to significant changes of GrIS including elevation changes up to 100 m. The sea level contribution estimated in this study may serve as a lower bound for RCP2.6 scenario, as the current observed observed sea level rise is in none of the experiments reached; this is attributed to processes not yet represented by the model but proven to play a major role in GrIS mass loss.

1 Introduction

Within the past decade the Greenland ice sheet (GrIS) has contributed by about 20% to sea level rise (Rietbroek et al., 2016) and global sea level rise has just recently shown to accelerate (Nerem et al., 2018). The mass loss of GrIS comprises two main contributions: acceleration of outlet glaciers and changes in the surface mass balance. In the past decades these changes in surface mass balance contributed to about 60%, whereas 40% is attributed to increasing discharge (van den Broeke et al., 2016). The question arises which impact the GrIS will have on global and regional sea level change in the next decades and centuries.

Negotiated during COP21, the Paris Agreement's aim is to keep a global temperature rise in this century well below 2°C above pre-industrial levels and to pursue efforts to limit the temperature increase even further to 1.5 degrees Celsius (UNFCCC, 2015). However, the statement holding global temperature below 2°C implies keeping global warming below the 2°C limit over the full course of the century and afterwards while efforts to limit the temperature increase to 1.5°C is often interpreted as allowing for a potential overshoot before returning to below 1.5°C (Rogelj et al., 2015). Here we selected the Representative Concentration Pathways (RCP, Moss et al., 2010) 2.6, being the lowest emission scenario considered within CMIP5 and in line with a 1.5°C or 2°C limit of global warming. Depending on the global circulation models (GCM) considered the global temperature change over time varies considerably although the political target is met at 2100. Whereas some models in RCP2.6 are not passing the limit of 1.5°C or 2.0°C global warming before 2100, other scenarios cross this limit and exhibit subsequent cooling (Frieler et al., 2017).

While global temperature rise may be limited to 1.5°C or 2°C by 2100, warming over Greenland is enhanced due to the Arctic amplification (Pithan and Mauritsen, 2014) and may exceed 4°C by that time and has exceeded 1.5°C (relative to 1951–1980) already in the past decade (GISTEMP Team, 2018). Given that this is about more than 2°C above the warming by 2000 this could have an considerable impact on ice sheet mass loss over Greenland. This implies an enlargement of the ablation zone and goes along with a decline in SMB. However, it is currently unclear, how fast GrIS could react to cooling and recovery of SMB, as ice sheets are also reacting dynamically to atmospheric forcing.

Recent large-scale ice sheet modelling attempts for projecting the contribution of the GrIS under RCP2.6 warming scenarios are very scarce. Fürst et al. (2015) conducted a very extensive study to simulate future ice volume changes driven by both atmospheric and oceanic temperature changes for all four representative concentration pathway scenarios. For the RCP2.6 scenario they estimate an abated sea level contribution of 42.3±18.0 mm by 2100 and 88.2±44.8 mm by 2300. The value by 2100 is in line with estimates given by the Fifth Assessment Report of the Intergovernmental Panel on Climate Change (IPCC AR5, IPCC (2013)). The AR5 range for RCP2.6 is between 10-100 mm by 2100 (the value is dependent whether ice-dynamical feedbacks are considered or not).

The GrIS response to projections of future climate change are usually studied with a numerical ice sheet model (ISM) forced with climate data. ISM response is subject to the dynamical part and the surface mass balance (SMB). In the past, ISMs often used the rather simple and empirical based positive degree day (PDD) scheme, in which the PDD index is used to compute melt, run-off and ice surface temperature from atmospheric temperature and precipitation (Huybrechts et al., 1991).

One disadvantage of the PDD method is, that the involved PDD parameters are tuned to correctly represent present-day melting rates but may fail to represent past or future climates (Bougamont et al., 2007; Bauer and Ganopolski, 2017). On one far end of model complexity, a regional climate model (RCM) resolves most processes at the ice-atmosphere interface and in the upper firn layers, such as RACMO (Noël et al., 2018) or MAR (Fettweis et al., 2017) with higher spatial and temporal resolution than GCMs. RCMs have been shown to be quite successful in reproducing the current SMB of the GrIS. However, as they are computationally expensive, an intermediate way would be most suitable, balancing computational costs and parameterisation of processes, such as the energy balance model of intermediate complexity, like SEMIC (Krapp et al., 2017).

Here we target in particular RCP2.6 peak and decline scenarios in order to study the GrIS response on overshooting by means with an numerical ISM. The projections are driven with climate data output from the CMIP5 RCP2.6 scenario provided by the ISIMIP2b project for different GCMs (Frieler et al., 2017). To obtain ice surface temperature and surface mass balance from the atmospheric fields, the surface energy balance model SEMIC (Krapp et al., 2017) is applied. The SEMIC model (Sect. 2.1) is driven offline to the ISM and therefore the climate forcing is one-way coupled and applied as anomalies to the ISM. The advantage of this one-way coupling is the lower computational costs, allowing for reasonably high spatial and temporal resolution of the ISM. In order to study the effect of overshooting, we design a RCP2.6-like scenario without an overshoot by manually stabilizing the forcing at 1.5°C.

For modelling the flow dynamics and future evolution of the GrIS under RCP2.6 scenarios, the thermo-mechanical coupled Ice Sheet System Model (ISSM, Larour et al., 2012) with a Blatter-Pattyn type higher order momentum balance (BP; Blatter, 1995; Pattyn, 2003) is applied (Sect. 2.5). A crucial prerequisite for projections is a reasonable initial state of the ice sheet in terms of ice volume, ice extent and ice surface velocities. Beside starting projections with the most realistic setting, the prevention of a model shock after switching from the initialization procedure to projections, is very important. Both has been a major issue in the past, which gave rise to an international benchmark experiment initMIP Greenland (Goelzer et al., 2018) for finding optimal strategies to derive initial states for the ice velocity and temperature fields. Using a hybrid approach of a thermal paleo-spin up and data assimilation has been shown to be a good way and is applied here.

Before driving the projections, the SMB forcing is validated thoroughly against RACMO. Then we explore the response of the GrIS and its contribution to sea-level rise under RCP2.6 scenario with overshoot and an modified RCP2.6 scenario without overshoot.

2 Model description

2.1 Energy Balance Model

Numerical ISMs need the annual mean surface temperatures and annual mean surface mass balance of ice as boundary conditions at the surface. To derive these ice sheet specific quantities, we use the surface energy balance model of intermediate complexity (SEMIC, Krapp et al., 2017). Although we only apply SEMIC and do neither adjust parameters of SEMIC, SEMIC is described very briefly. SEMIC computes the mass and energy balance of snow and/or ice surface. In order to tune parameters for a number of processes, (Krapp et al., 2017) performed an optimisation based on reconstruction and regional climate model data. These parameters have been used in our study, too. The energy balance equation reads as

$$c_{\text{eff}} \frac{\mathrm{d}T_{\mathrm{s}}}{dt} = (1-\alpha) \cdot \mathrm{SW}^{\downarrow} - \mathrm{LW}^{\uparrow} + \mathrm{LW}^{\downarrow} - H_{\mathrm{S}} - H_{\mathrm{L}} - Q_{\mathrm{M/R}}, \tag{1}$$

where α is the surface albedo that is parameterized with the snow height (Oerlemans and Knap, 1998). The downwelling shortwave $\mathrm{SW}^{\downarrow}$ and downwelling longwave radiation $\mathrm{LW}^{\downarrow}$ at the surface are provided as atmospheric forcing (sect. 2.2). The upwelling longwave radiation $\mathrm{LW}^{\uparrow}$ is described by the Stefan-Boltzmann law. The latent H_{L} and sensible H_{S} heat fluxes are estimated by the respective bulk approach (e.g. Gill, 1982). The residual heat flux $Q_{\mathrm{M/R}}$ is calculated from the difference of melting M and refreezing R and keeps track of any heat flux surplus or deficit in order to keep the ice surface temperature T_{s} below or equal to 0°C over snow and ice.

The surface mass balance SMB in SEMIC is considered as follows

$$\mathrm{SMB} = P_{\mathrm{s}} - SU - M - R, \tag{2}$$

where P_{s} is the rate of snowfall and SU the sublimation rate, which is directly related to the latent heat flux. The melt rate is dependent on the snow height, if all snow is melted down the excess energy is used to melt the underlying ice. Refreezing is calculated differently for available melt water or rainfall. Moreover, the porous snowpack could retain a limited amount of meltwater while over ice surfaces refreezing is neglected and all melted ice is treated as run-off. In SEMIC, the total melt rate M and refreezing rate R are calculated from available energy during the course of one day. As the set of equations are solved using an explicit time-step scheme with a time step of one day, a parametrization for the diurnal cycle (a cosine function) account for thawing and freezing over a day. This reduced complexity, one-layer snowpack model saves computation time and allows for integrations on multi-millennial timescales compared to more sophisticated multilayer snowpack models. Further details are given by Krapp et al. (2017).

2.2 Atmospheric forcing

Here we targeted in particular peak and decline scenarios, temporarily exceeding a given temperature limit of global warming to 2.0°C or even 1.5°C by the end of 2100. From the official extended RCP2.6 scenarios (Meinshausen et al., 2011), we have selected GCMs which covering the CMIP5 historical scenario, the RCP2.6 scenario until 2299 and reveal an overshoot in annual global mean near-surface temperature change relative to pre-industrial levels (1661–1860). Three different GCMs were used in our study: IPSL-CM5A-LR (L'Institut Pierre-Simon Laplace Coupled Model, version 5 (low resolution)), MIROC5 (Model for Interdisciplinary Research on Climate, version 5) and HadGEM2-ES (Hadley Centre Global Environmental Model 2, Earth System). The GCM output was provided and prepared by the ISIMIP2b project following a strict simulation protocol (Frieler et al., 2017). Figure 1a displays the temporal evolution of the annual global mean near-surface air temperature T_{a} for those GCMs for the historical simulation up to 2005 continued with the RCP2.6 simulation up to 2299. Global-mean-temperature projections from IPSL-CM5A-LR and HadGEM2-ES under RCP2.6 exceed 1.5°C relative to pre-industrial levels in the second half of the 21$^{\mathrm{st}}$ century. While global-mean-temperature change returns to 1.5°C or even slightly lower by 2299 in HadGEM2-ES, it only reaches about 2°C in IPSL-CM5A-LR by 2299. For MIROC5, it stabilizes at about 1.5°C during the second half of the 21$^{\mathrm{st}}$ century. In order to determine the onset of overshoot we scan the historical and RCP2.6 scenarios of the individual GCMs identifying the time, when the global warming reaches 1.5°C in a 11-year moving window above pre-industrial levels. The characteristic dates of overshooting 1.5°C for HadGEM2-ES is by 2021; MIROC5 reaches this level by 2041, while IPSL-CM5A-LR by 2009 (coloured dots in Fig. 1).

The phenomenon, that tends to produce a larger change in temperature near the poles was termed polar amplification. Particularly, it enhances the increase in global mean air temperature over arctic areas (referred here as arctic amplification). Generally, the the CMIP5 models show an annual average warming factor over the Arctic between 2.2 and 2.4 times the global average warming (IPCC, 2013, Tab. 12.2). As mechanisms creating the arctic amplification may be represented to different extents in the GCMs, the level of future amplification is different across the GrIS. The three GCMs used in this study represent this trend to differing extents over GrIS[1] (Fig. 1 and 2). For HadGEM2-ES and IPSL-CM5A-LR the arctic compared to the global warming is amplified relatively similar (warming approx. 4°C relative to 1661–1860). In contrast, MIROC5 reveals a considerably lower arctic amplification (warming approx. 3°C relative to 1661–1860). A striking feature among all models is the higher variability over GrIS compared to the global mean values. In terms of global and arctic future annual mean near-surface temperatures MIROC5 is the lowest and IPSL-CM5A-LR the highest forcing.

The ISIMIP2b atmospheric forcing data are CMIP5 climate model output data that have been spatially interpolated to a regular 0.5°×0.5° latitude-longitude grid and bias-corrected using the observational dataset EWEMBI (Frieler et al., 2017; Lange, 2017). To drive the SEMIC model to obtain the ice surface temperature T_{s} of the ice sheet and the surface mass balance SMB we need to provide the atmospheric forcing (consisting of incoming shortwave radiation $SW^{\downarrow}$, longwave radiation $LW^{\downarrow}$, near-surface air temperature T_{a}, surface wind speed u_{s}, near-surface specific humidity q_{a}, surface air pressure p_{s}, snowfall rate P_{s}, and rainfall rate P_{r}). These fields are available from the three GCMs model output data. SEMIC is driven by the daily input of the GCMs while the output is a cumulative surface mass balance and a mean surface temperature over each year.

Given the differences in resolution between the GCMs and ISSM, a vertical downscaling procedure is applied to the atmospheric forcing fields. First the atmospheric fields are conservatively interpolated from the GCM grid onto a regular high resolution 0.05° grid. The output fields of SEMIC are subsequently conservatively interpolated on the unstructured ISSM grid. This two-step procedure is not necessary but currently it is technical the easiest way. For future applications we will avoid the intermediate interpolation and run SEMIC directly on the target unstructured ISSM grid.

To account for the difference in ice sheet surface topography between GCMs and ISSM corrections for several quantities $(\cdot)$ denoted by $(\cdot)^{\mathrm{cor}}$ are initially performed. We follow the corrections proposed by Vizcaíno et al. (2010)

$$(\cdot)^{\mathrm{cor}} = (h_s^{\mathrm{SEMIC}} - h_s^{\mathrm{GCM}})\gamma_{(\cdot)}, \tag{3}$$

with the lapse rates $\gamma_{(\cdot)}$ shown in Table 1 and h_s^{SEMIC} is equal the ISSM ice surface elevation at the initial state. Subsequently, SEMIC computes the ice-surface temperature T_{s} and the surface mass balance SMB based on these corrected input values.

[1]For all occurrences, the GrIS is defined as the ice mask provided from BedMachine Greenland (Morlighem et al., 2014).

Table 1. Lapse rates and height-desertification relationship for initial corrections of GCM output fields near-surface air temperature T_a, precipitation of snow P_s, precipitation of rain P_r, and downwelling longwave radiation $LW^{\downarrow}$ used as input for SEMIC. Here, h^{ref} = 2000 m and $\gamma_p = -0.6931\,\mathrm{km}^{-1}$ is the desertification coefficient.

variable	lapse rate γ and desertification relationship	reference
T_a	0.74 K/100 m	Erokhina et al. (2017)
$LW^{\downarrow}$	$2.9\,\mathrm{W\,m^{-2}}$	Vizcaíno et al. (2010)
P_s, P_r	$\exp(\gamma_p[\max(h_s^{\mathrm{ISSM-pd}}, h^{\mathrm{ref}}) - h^{\mathrm{ref}}]) \quad \forall \quad h_s^{\mathrm{GCM}} \leq h^{\mathrm{ref}}$	Vizcaíno et al. (2010)
P_s, P_r	$\exp(\gamma_p[\max(h_s^{\mathrm{ISSM-pd}}, h^{\mathrm{ref}}) - h_s^{\mathrm{GCM}}]) \quad \forall \quad h_s^{\mathrm{GCM}} > h^{\mathrm{ref}}$	Vizcaíno et al. (2010)

SEMIC is applied as developed by Krapp et al. (2017). These authors perform a particle-swarm optimization to calibrate model parameters for the GrIS and validate them against the RCM MAR. We adopt their derived parameters here. The parameter tuning aimed to find a parameter set which gives a best fit between SMB and ice temperature T_{s} of SEMIC with only a limited number of processes and simpler parameterisations compared to a more complex RCM. A RCM is typically validated against reanalysis data and observations, therefore, we assume the tuned parameters are most reliable to represent the processes and parametrizations within SEMIC. In terms of process description the optimized SEMIC configuration leads to the best possible SMB and T_{s} fields. However, although the coarse GCM-based forcing has underwent a downscaling of particular fields and is processed in SEMIC with a higher resolution the atmospheric fields over the ice sheet still lacks details and quality compared to a RCM. Given the experiences we made with GCMs used in this study (e.g. the timing of maximum warming, the length of an overshoot) would require a separate tuning for each GCM. This basically means to compensate, for e.g. too low near surface temperatures, with SEMIC parameters, which would offset the whole comparison of GCM forcing. Furthermore, this additional tuning steps would make the benefit of having a semi-complexity model with low costs meaningless.

Because the details of the GrIS surface climate are not well captured on the GCM coarse grid, the absolute SEMIC output fields (SMB and T_{s}) are not directly used to force the numerical ice flow model ISSM. The climatic boundary conditions applied here consist of a reference field onto which climate change anomalies from SEMIC are superimposed. The initialization of the ice flow model based on data assimilation makes it possible to use forcing data from high resolution RCMs that were run on the same ice sheet mask and ice surface topography. As the reference SMB field we choose the downscaled RACMO2.3 product (Noël et al., 2018) whereby a model output was averaged for the time period 1960–1990, denoted $\overline{\mathrm{SMB}}(1960-1990)_{\mathrm{RACMO}}$. The reference period 1960–1990 is chosen ice sheet is assumed close to steady state in this period (e.g. Ettema et al., 2009). The climatic SMB that is used as future climate forcing read as

$$\mathrm{SMB}_{\mathrm{clim}}(x,y,t) = \overline{\mathrm{SMB}}_{\mathrm{RACMO}}^{(1960-1990)}(x,y) + \Delta\mathrm{SMB}(x,y,t), \tag{4}$$

with the anomaly defined as

$$\Delta\mathrm{SMB}(x,y,t) = \mathrm{SMB}_{\mathrm{SEMIC}}(x,y,t) - \overline{\mathrm{SMB}}_{\mathrm{SEMIC}}^{(1960-1990)}(x,y), \tag{5}$$

where t={1960, 1961, ... , 2299}. Note that the historical scenario is run from 1960–2005 and followed by the RCP2.6 scenario from 2006–2299. In an ideal case, both reference terms $\overline{\mathrm{SMB}}(1960-1990)_{\mathrm{RACMO}}$ and $\overline{\mathrm{SMB}}(1960-1990)_{\mathrm{SEMIC}}$ will cancel out and the absolute climatic forcing $\mathrm{SMB}_{\mathrm{SEMIC}}(x,y,t)$ would remain. This is certainly not the case and the equation must be interpreted as having the RACMO reference field (with a good spatial distribution) as a background field with the trends from SEMIC superimposed.

The same equations hold for the temperature imposed on the ice-surface. This ensures that the unforced control experiment produces identical behaviour for each GCM. Results for future projections depend only on the atmospheric GCM input, or similarly SEMIC output, and therefore the results can be compared quantitatively.

In the presented study, the ice flow model is forced with the offline processed SEMIC output. This one-way coupling strategy is computational cheaper and the technically challenging online coupling is avoided. However, as the ice sheet evolves in response to climate change, local climate feedback processes are not captured. Most importantly the interaction of the ice surface between air temperature and precipitation, which in turn affects the surface mass balance. The SMB-feedack process is considered with a dynamic correction to the $\mathrm{SMB}_{\mathrm{clim}}$ (see sect. 2.7 below). This correction is applied within ISSM and to the surface mass balance term only.

2.3 Validation of SMB forcing

In order to validate the obtained climatic $\mathrm{SMB}_{\mathrm{clim}}$ (Eq. 4), the resulting SMB patterns and time series are compared with other available data-sets. Beside the spatial pattern of the surface mass balance, the time series of the integrated SMB over Greenland illustrate what the ice sheet's total surface gains and losses have been over the year from SMB (Fig. 3). The grey shaded box and black line depicts the range and the mean SMB between 1981–2010 from Polarportal (polarportal.dk) derived from a combination of observations and a weather model for Greenland (Hirlam-Newsnow). The dashed black line shows the results from the RACMO2.3 product. The integrated SMB magnitude of each GCM is consistent with RACMO2.3 and polarportal data. The drop in SMB after 2000 is present in all three GCMs and RACMO. The decline of SMB roughly corresponds with MAR results forced with the GCM NorESM1-M under RCP2.6 scenario (Fettweis et al., 2013, last column in Tab. 2), although it is not strictly comparable because they use a different GCM climate data. They estimated a loss of -124±100 Gt a^{-1} in 2080–2099 relative to 1980–1999.

For HadGEM2-ES the integrated SMB remains around 200 Gt a^{-1} after 2050. The SMB for IPSL-CM5A-LR recovers from 2050 onwards and shows an increase from around 200 Gt a^{-1} to around 350 Gt a^{-1} by 2300. MIROC5 reveals the lowest SMB change over time and recovers after 2050 from 250 Gt a^{-1} to 300–350 Gt a^{-1} by 2300. The SMB of IPSL-CM5A-LR and MIROC5 is by 2300 almost of similar magnitude as present-day.

For the available RACMO2.3 time series we have computed the coefficient of determination r^2 and the mean signed difference (MSD) for surface mass balance, accumulation and melt (Fig.4). The interannual SMB variability agrees well and the MSD oscillates around zero and with values up to ±0.5 m a^{-1} (Fig.4a). For the time period 1960–2016 the overall surface mass balance difference over the ice sheet between SEMIC and RACMO is almost zero with -0.007 m a^{-1}, 0.016 m a^{-1} and 0.0200 m a^{-1} for HadGEM2-ES, IPSL-CM5A-LR and MIROC5, respectively. These numbers are in the same range as given

Table 2. Annual mean integrated SMB ($\mathrm{Gt\,yr^{-1}}$) covering various periods. Time series of $\mathrm{SMB_{clim}}$ for the GCMs are calculated by Eq. 4 for RCP2.6 scenario with overshoot. The column '1.5°C reached' gives an 11-year mean at the characteristic time of overshooting 1.5°C. Anomaly in SMB (ΔSMB) is in 2080–2099 with respect to 1980–1999.

Model	1960–1990	1960–1997	1997–2016	1981–2010	1960–2016	1.5°C reached	ΔSMB
RACMO2.3	402.8	403.4	279.1	363.1	364.8	-	-
polarportal	-	-	-	370	-	-	-
MAR [a]	-	-	-	-	-	-	-124 ± 100
HadGEM2-ES	400.0	391.2	277.0	358.1	355.2	170.0	-179.2
IPSL-CM5A-LR	408.9	412.5	332.8	403.7	382.2	363.9	-170.4
MIROC5	395.0	398.5	341.2	341.8	380.0	288.4	-80.9

[a] MAR forced with GCM NorESM1-M under RCP2.6 scenario (Fettweis et al., 2013)

by Krapp et al. (2017) for the comparison between SEMIC and MAR. Nonetheless, averaging the MSD over the whole time period the surface accumulation agrees better compared to surface melt (surface accumulation: -0.034 $\mathrm{m\,a^{-1}}$, -0.031 $\mathrm{m\,a^{-1}}$, -0.023 $\mathrm{m\,a^{-1}}$; surface melt: 0.048 $\mathrm{m\,a^{-1}}$, 0.066 $\mathrm{m\,a^{-1}}$, 0.061 $\mathrm{m\,a^{-1}}$). The coefficient of determination is larger than 0.8 for all components except with some outliers.

Table 2 shows annual mean integrated SMB over the entire GrIS for various periods. Averaged over most of the periods the annual mean integrated SMB is among the model rather similar. Most obvious are the differences between the GCMs for the period 1997–2016. The year 1997 was identified as the critical time of Greenland's peripheral glaciers and ice caps mass balance decrease (Noël et al., 2017). For this period of declining SMB the HadGEM2-ES agrees well to the RACMO2.3 product. In general the compared values over all time periods agree fairly well.

The validation include an analysis of the spatial pattern of SMB. Here we compare exemplary the spatial pattern of RACMO2.3 for the year 1990 against the SMB derived from HadGEM2-ES for the year 1990 (Fig. 5). The maps show, that accumulation and ablation patterns agree reasonably well. The SMB patterns for other GCMs or time slices are qualitatively similar but deviate in absolute values as the annual variability is not coherent among all models.

2.4 Modified RCP2.6 scenario without overshoot

The global climate warming of the selected GCMs exceeds the political target of 1.5°C during the 20^{th} century although the RCP2.6 is the strongest mitigation scenario focussing on negative emissions (Moss et al., 2010). In order to estimate the overshooting effect on the projected sea level contribution from the GrIS we manually construct a RCP2.6-like scenario without an overshoot assuming an immediate climate stabilisation at that time when 1.5°C is reached. As mentioned before, we identify the time when the global warming reaches 1.5°C in a 11-year moving window above pre-industrial levels. The characteristic times of overshooting 1.5°C for HadGEM2-ES is by 2021; MIROC5 reaches this level by 2041, while IPSL-CM5A-LR by 2009. Before reaching these threshold the unaltered historical and RCP2.6 forcing is applied. The extension of the forcing from these characteristic times is of crucial importance. Since the forcing is constructed by using the GCM trends instead of absolute values an arbitrary time period can be used. In order to account for decadal variability and assuming a stabilized climate we reuse the climatic forcing fields from 2250–2280 until the end of the simulation (light grey shaded areas in Fig. 1 and 3). At the characteristic times the three GCMs reveal a SMB that differs up to 200 $\mathrm{Gt\,yr^{-1}}$ (Column '1.5°C reached' in Tab. 2). While HadGEM2-ES has declined to 170 $\mathrm{Gt\,yr^{-1}}$, IPSL-CM5A-LR remains with 363.9 $\mathrm{Gt\,yr^{-1}}$ relatively close to present-day. In the following, the modified RCP2.6-like scenario without overshoot is termed as RCP2.6 without overshoot.

2.5 Ice flow model

Ice flow and thermodynamic evolution of the GrIS are approximated using the finite-element ISSM. The model has been applied successfully to both large ice sheets (Bindschadler et al., 2013; Nowicki et al., 2013; Goelzer et al., 2018) and is also used for studies of individual drainage basins of Greenland, e.g. the North East Greenland Ice Stream (Choi et al.), Jakobshavn Isbræ (Bondzio et al., 2016, 2017) and Store Glacier (Morlighem et al., 2016). Here, we use an incompressible non-Newtonian constitutive relation with viscosity dependent on temperature, microscopic-water content and strain rate, while neglecting the softening effect of damage or impurities. The BP approximation to the Stokes momentum balance equation is employed in order to account for longitudinal and transverse stress gradients.

ISSM is specified with kinematic boundary conditions at the upper and lower boundary of the ice sheet. The upper boundary incorporates the climatic forcing, i.e. the surface mass balance and ice surface temperature, while the base of the ice is specified as both impenetrable with the bedrock and in balance with the rate of melting. The basal melt rate below ice shelves is parameterised with a Beckmann-Goosse relationship (Beckmann and Goosse, 2003). The melt-factor is roughly adjusted such that melting rates corresponds to literature values (e.g. Wilson et al., 2017). Within this study the basal melt rate is not a focus and hence the basal melt underneath floating tongues or vertical calving fronts of tidewater glaciers are not changed. Once the pressure melting point at the grounded ice is reached melting is calculated from basal frictional heating and the heat flux difference at the ice/bed interface At the ice base sliding is allowed everywhere and the basal drag, $\boldsymbol{\tau}_b$, is written using Coulomb friction:

$$\boldsymbol{\tau}_b = -k^2 N \boldsymbol{v}_b, \tag{6}$$

where $\boldsymbol{v}_b$ is the basal velocity vector tangential to the glacier base and k^2 a constant. The effective pressure is defined as $N = \varrho_i\, g\, H + \varrho_w\, g\, h_b$, where H is the ice thickness, h_b the glacier base and $\varrho_i = 910\,\mathrm{kg\,m^{-3}}$, $\varrho_w = 1028\,\mathrm{kg\,m^{-3}}$ the densities for ice and sea water, respectively. We apply water pressure at marine terminating glaciers and observed surface velocities (Rignot and Mouginot, 2012) at land terminating glaciers. A traction-free boundary condition is imposed at the ice/air interface.

Geothermal heat flows into the ice in contact with bedrock and adjust dynamically to the thermal state of the base (Aschwanden et al., 2012; Kleiner et al., 2015). The spatial pattern of the geothermal flux is taken from Greve (2005, scenario hf_pmod2). The ice surface temperature includes Dirichlet conditions from the atmospheric forcing explained above.

For all simulations, the ice front is fixed in time, and a minimum ice thickness of 10 m is applied. This implies that calving exactly compensates the outflow through the margins and initially glaciated points are not allowed to become ice-free. However, regions that reach this minimum thickness are assumed to retreat. The grounding line is allowed to evolve freely according to a sub-grid parameterization scheme, which tracks the grounding line position within the element (Seroussi et al., 2014).

Model calculations are performed on a horizontally unstructured grid with a higher resolution, $l_{\min} = 1\,\mathrm{km}$, in fast flow regions and coarser resolution, $l_{\max} = 20\,\mathrm{km}$, in the interior. The vertical discretisation comprises 15 layers refined towards the base where vertical shearing becomes more important. The complete mesh comprises 574 056 elements. Velocity, enthalpy (i.e. temperature and microscopic water content) and geometry fields are computed on each vertex of the mesh using piecewise-linear finite elements. The Courant-Friedrichs-Lewy condition (Courant et al., 1928) dictates a time step of 0.025 years. Using the AWI cluster Cray-CS 400 computer, a simulation with an integration time of 340 years requires ≈ 8 hours on 16 nodes comprised of 36 CPUs.

2.6 Initial state

Future projections of ice sheet evolution first require the determination of the initial state. Different methods are currently used to initialize ice sheets and it has been shown, that the initial state is crucial for projections of ice dynamics (Bindschadler et al., 2013; Nowicki et al., 2013; Goelzer et al., 2018). The recent initMIP-GrIS intercomparison effort (Goelzer et al., 2018) focusses on the different initialization techniques applied in the ice flow modelling community and found none of them is the method of choice in terms of a good match to observations and a long term continuity. All methods are required for modelling the projections of the GrIS planned within CMIP6 phase (Nowicki et al., 2016) on time scales up to a few hundred years. However, while inverse modelling is well established for estimating basal properties, the temperature field is difficult to constrain without performing an interglacial thermal spin-up.

Here, we setup a hybrid approach between spin-up and inversion scheme to estimate the initial state. The ice sheet geometry (bed, ice thickness and ice sheet mask) is taken from the mass-conserving BedMachine Greenland data set (Morlighem et al., 2014). The geometric input for thickness and ice sheet mask are masked to exclude glaciers and ice caps surrounding the ice sheet proper. An initial relaxation run over 50 years assuming no sliding and constant ice temperature of -20°C is performed to avoid spurious noise. A temperature spin-up is then performed using this time-invariant geometry. As the computational expensive BP approximation is employed, mesh refinements are made at certain points during the whole initialization procedure (see Table 3). The first mesh sequence is starting 125 kyr before 1990 and run up to the year 1960 and assumes a spatially constant friction coefficient $k^2 = 50\,\mathrm{s\,m^{-1}}$ and forced with paleo-climatic conditions. The imposed paleo-climatic conditions is a multi-year mean from the years 1960 to 1990 of the RACMO2 product (Ettema et al., 2009) and offset by a spatially constant surface temperature anomaly for the last 125 kyr based on the GRIP surface temperature history derived from the $\Delta^{18}O$ record (Dansgaard et al., 1993). The initial ice temperature at 125 kyr before 1990 is a steady-state temperature distribution taken from a spin-up with time independent climatic conditions from the reference period 1960–90. The spin-up is done to 1960 in order to start the projections before the critical time of Greenland's peripheral glaciers mass balance decrease (Noël et al., 2017) with an additional buffer of approx. 30 years.

In the subsequent basal-friction inversion, the ice rheology is kept constant using the enthalpy field from the end of the temperature spin-up. The inversion approach infers the basal friction coefficient k^2 in Eq. 6 by minimizing a cost function

Table 3. Mesh Statistics.

mesh sequence	$l_{\min}$ (km)	$l_{\max}$ (km)	number of elements	integration time in thermal spin-up (kyr)
1	15	50	117 586	125
2	5	50	192 220	125
3	2.5	35	272 650	25
4	1	20	574 056	15

that measures the misfit between observed and modelled horizontal velocities (Morlighem et al., 2010). Observed horizontal surface velocities are taken from (Rignot and Mouginot, 2012). The procedure of temperature spin-up and inversion is repeated on the subsequent three mesh sequences. The repeated temperature spin-ups starting 125 kyr, 25 kyr and 15 kyr before 1990 and again run up to the year 1960. The initial values for the temperature field at these times are taken from the respective times from the previous mesh sequence; the basal-friction coefficient is updated from the inversion on the previous mesh sequence. The mesh sequencing reduces the expense of initialization and produces a sufficiently consistent result in terms of velocity and enthalpy. Note that mesh sequence 1-3 are only used during initialization while the final solution of mesh sequence 4 at year 1960 of this procedure is used as initial state for all projections presented below.

For the hybrid initialization we make the three basic assumptions: (1) The currently observed present-day elevation is valid for the entire glacial cycle: changes in elevation and spatial extent of the GrIS are ignored, (2) the basal friction coefficient obtained from the inversion is valid for the past glacial cycle, and (3) the GRIP record can be applied to the whole ice sheet without spatial variations.

Please note, that similar results from this procedure have been submitted to the ISMIP6 initMIP-Greenland effort (Goelzer et al., 2018), but the simulations were run with the geothermal flux distribution by Shapiro and Ritzwoller (2004) and additionally with a time independent climate forcing representing present-day conditions. However, by using the modified heat-flux distribution by Greve (2005, scenario hf_pmod2) we found a generally better agreement to measured basal temperatures at ice core locations. Basically, the comparison of simulated to observed temperatures at the ice base shows too low temperatures for some locations. Due to the fact, that the applied inversion technique for the friction coefficient allows sliding everywhere, the portion of deformational shearing may be underestimated, which cannot be proven without any observations of basal velocities that are unfortunately not existing at all. However, for our projections on centennial timescales this is a negligible effect (Seroussi et al., 2013).

2.7 Synthetic and dynamic surface mass balance parameterization

As we perform a one-way coupling of the climatic forcing the SMB-elevation feedback needs to be considered. Here we rely on the dynamic SMB parameterization developed by Edwards et al. (2014a, b) and previously applied by Goelzer et al. (2013).

This parameterization assumes that the effect of SMB trends follow a linear relationship

$$\mathrm{SMB}_{\mathrm{dyn}}(x,y,t) = \mathrm{SMB}_{\mathrm{clim}}(x,y,t) + b_i(h_s(x,y,t) - h_{\mathrm{fix}}(x,y)), \tag{7}$$

where $\mathrm{SMB}_{\mathrm{dyn}}(x,y,t)$ and $\mathrm{SMB}_{\mathrm{fix}}(x,y,t)$ are the SMB values with and without taking height changes into account, respectively. The surface elevation changes are taken from ISSM elevation $h_s(x,y,t)$ while running the simulation and a reference elevation $h_{\mathrm{fix}}(x,y)$. In our setup the reference elevation correspond to the ISSM ice surface elevation at the initial state.

In this parameterization the SMB gradient b_i is dependent of both location and sign. It can take four values and a separation is made on the location relative to 77°N and on the sign of the SMB. This separates regions of largely different sensitivity, namely the ablation zone with a larger gradient compared to the accumulation zone, and a more sensitive ablation zone in the South compared to the North. While a complete uncertainty analysis is given by Edwards et al. (2014a), only the maximum likelihood gradient set, $\boldsymbol{b} = (b_p^N, b_n^N, b_p^S, b_n^S)$, is used here:

$$\begin{aligned}
b_p^N =& 0.085\,\mathrm{kg\,m^{-3}\,a^{-1}},\\
b_n^N =& 0.543\,\mathrm{kg\,m^{-3}\,a^{-1}},\\
b_p^S =& 0.063\,\mathrm{kg\,m^{-3}\,a^{-1}},\\
b_n^S =& 1.890\,\mathrm{kg\,m^{-3}\,a^{-1}},
\end{aligned}$$

where the subscripts (p,n) and the superscripts (N,S) indicate the evaluation of the SMB sign and the region separation, respectively.

A shortcoming of the performed hybrid initialization is, that usually a fixed initial ice sheet causes a model drift when imposing the ice thickness equation. This is a result from using an ice sheet that is not in equilibrium with the applied SMB and ice flux divergence. We utilize the local ice thickness imbalance once the ice sheet is released from its fixed topography from an one year unforced relaxation run, i.e. $\Delta\mathrm{SMB}(x,y,t) = 0$ in Eq. 5. The resulting $\partial H/\partial t$ is subtracted as a surface mass balance correction, $\mathrm{SMB}_{\mathrm{corr}}(x,y)$, for the further runs (similar as in Price et al. (2011); Goelzer et al. (2018)). However, instead of assuming an zero SMB anomaly one could calculate the anomaly with a GCM input from the CMIP5 pre-industrial scenario. But given the small temperature changes the SMB anomaly will be close to zero and the calculated ice thickness imbalance is unlikely affected by it. However, the final SMB correction is on average 0.01 $\mathrm{m\,a^{-1}}$, with 5% of the total ice-sheet area having a correction of >25 $\mathrm{m\,a^{-1}}$, predominantly at marine-terminated ice margins and ice streams (Fig. 6). For these locations the synthetic SMB correction can be considered as an additional ice thinning or thickening from dynamic discharge that is not intrinsically simulated. A performed control run with the imposed SMB correction exhibits a negligible model drift in terms of sea level equivalent (SLE, black dashed line in Fig. 9 and section 3.2).

The final surface mass balance that the numerical ice flow model sees is composed of several components

$$\mathrm{SMB} = \mathrm{SMB}_{\mathrm{clim}}(x,y,t) - \mathrm{SMB}_{\mathrm{corr}}(x,y) + \mathrm{SMB}_{\mathrm{dyn}}(x,y,t)\,. \tag{8}$$

3 Results

3.1 Present day elevation and velocities

Figure 7 displays exemplary the observed and simulated velocities for the year 2000 (defined here as present day) after a period of forcing with HadGEM2-ES from 1960 onwards. The resulting horizontal velocity field captures all major features well, including the North East Greenland Ice Stream (NEGIS). Outlet glaciers terminating in narrow fjords in the southeastern region are resolved, however, slow moving areas tend to retreat below minimum ice thickness and with that the ice extent in this area is underestimated. However, ice surface elevations agree fairly well (Fig. 8a). In general large outlet glaciers like Kangerdlusuaq, Helheim and Jakobshavn Isbræ reveal lower velocities in their fast termini that reflects the high RMS of about $390\,\mathrm{m\,a^{-1}}$ (Fig. 8b). Compared to the low RMS values of $<20\,\mathrm{m\,a^{-1}}$ for the AWI-ISSM results on the regular 5 km grid given in Goelzer et al. (2018), the analysis here was done on the original native grid with the high resolution in fast flow regions and on other hand the model was already run forward in time.

3.2 Projections of mass change

After passing the assumed critical time of decreasing SMB of GrIS and the present day state, the ice sheet experienced a warming and associated mass loss from surface mass balance. Projections of the evolution of SLE of the ice sheet under RCP2.6 scenario with overshoot until 2100 and 2300 are shown in Fig. 9 for each GCM (straight lines) and Table 4. The simulated volume above floatation is converted into the total amount of global sea level equivalent (SLE) by assuming an ocean area of about $3.618\times10^{8}\,\mathrm{km}^{2}$. Although the control run shows a negligible model drift in terms of SLE, the RCP2.6 projected SLE is corrected by the control run. By 2100, the model range of Greenland sea-level contributions is between 21.3 and 38.1 mm with an average of 27.9 mm and by 2300 between 36.2 and 85.1 mm with and average of 53.7 mm. Compared to Fürst et al. (2015) our mean values are lower but still in their model variability.

The evolution of the mass change is showing distinct behaviours: between 1960–2000 almost no change for HadGEM2-ES and IPSL-CM5A-LR while MIROC5 is gaining mass; a change in trend with a minor increase between 2000–2015 and a steep increase from then on for HadGEM2-ES and IPSL-CM5A-LR; SLE increase for MIROC5 is more gently. The steep rise in SLE for HadGEM2-ES and IPSL-CM5A-LR is linked to the steep reduction in SMB for both models at the same time. The kink of SLE in HadGEM2-ES and IPSL-CM5A-LR around 2050 is caused by a positive SMB anomaly (compare Fig. 3). Also MIROC5 represents this peak in SMB, however slightly later, around 2060. These short-term drops in SLE are linked to positive anomalies in SMB. For HadGEM2-ES the ice sheet contribution until 2300 generally increases continuously while for IPSL-CM5A-LR and MIROC5 the increase levels off. This is an intriguing effect as HadGEM2-ES and IPSL-CM5A-LR are showing in terms of warming over GrIS a similar behaviour (Fig. 1). In fact, the SMB of IPSL-CM5A-LR recovers from 2050 onwards (Fig. 3), while the SMB of HadGEM2-ES remains on a low level

For the RCP2.6 scenario without overshoot the behaviour of SLE for HadGME2-ES is similar but with lower values. The SLE for MIROC5 is by 2100 approx. 5 mm lower but approaches the same value at 2300 without attaining a pronounced plateau. A striking feature is the much lower SLE estimated from IPSL-CM5A-LR which never exceeds a value of 10 mm and

Table 4. Contribution of the Greenland ice sheet to global sea-level change by 2100 and 2300 in mm SLE under RCP2.6 scenario with and without overshoot.

Model / Study	2100 with overshoot	2100 without overshoot	2300 with overshoot	2300 without overshoot
HadGEM2-ES	38.1	29.6	85.1	66.9
IPSL-CM5A-LR	24.4	7.5	36.2	3.4
MIROC5	21.3	15.0	39.9	40.9
Average	27.9	17.4	53.7	37.1
Fürst et al. (2015)	42.3±18.0	-	88.2±44.8	-

gains mass about 2225 onwards. The average SLE from all three GCMs is 17.4 mm by 2100 and 37.1 mm by 2300, that is approximately one third less compared to the RCP2.6 scenario with overshoot.

The observed sea level contribution between 2002 and 2014 is 0.73 mm a^{-1} (Rietbroek et al., 2016). In the same period the simulated contribution is only 0.16 mm a^{-1} for HadGEM2-ES, 0.17 mm a^{-1} for IPSL-CM5A-LR and lowest for MIROC5 with 0.13 mm a^{-1}. In order to assess a potential temporal lag between simulated and observed value, mean values of similar periods are calculated (Fig. 10). None of the models reach the observed value; HadGEM2-ES reaches a maximum value of 0.59 mm a^{-1} 13 years later; IPSL-CM5A-LR a value of 0.48 mm a^{-1} 12 years later and MIROC5 a value of 0.36 mm a^{-1} 40 years later. For the RCP2.6 scenario without overshoot, the values are smaller.

3.3 Future climatic forcing fields

For the different GCMs used we compute ice surface temperature T_s differences between 2100/2300 and 2000 as a multi-year mean over five years do reduce the inter-annual variability (Fig. 11). HadGEM2-ES leads to an increase in temperatures along the northern margins by up to 4°C. By 2100 the Western areas and vast majority of the ice sheet exceed 2°C of warming. The only pronounced warming by 2300 is in the Northwestern regions, while the ice sheet surface temperatures decrease from 2100. IPSL-CM5A-LR exhibits a significantly different pattern. This simulation produces pronounced warming in the center (up to 3°C) and in the Southeast (up to 4°C) of the ice sheet, while the Northern areas are only moderately warming around 1°C during the 20^{th}. The pattern is similar in 2300, with a cooling in the West. The cooling after 2100 is by far less than in HadGEM2-ES. The least warming is found in MIROC5, which even exhibits cooling in the southern areas by about -1°C and +1°C is only reached in 2100 in the North. By 2300 the entire ice sheet experiences warming; however this warming is quite moderate compared to the other two GCMs. The low magnitude of warming compared to global warming let us infer that the mechanisms of arctic amplification is not well represented in MIROC5.

Although we do not have a measure to judge future climate warming trends, but with respect to the Arctic amplification phenomena the most plausible distribution of surface warming is produced by HadGEM2-ES and MIROC5, while only HadGEM2-ES also reaching a plausible magnitude of warming with overshooting the global mean values. IPSL-CM5A-LR is spatially and temporally experiencing the largest warming; however, the distribution is not in agreement with the Arctic amplification. However, the assessment of the GCMs is in line with skill tests performed by Watterson et al. (2014). They assigned skill cores by comparing individual GCM output data against re-analysis data. The analysis indicates that all 25 models have a substantial degree of skill, however, HadGEM2-ES is ranked in the top, MIROC5 in the middle, and IPSL-CM5A-LR in lower part.

Figure 12 presents in a similar fashion as Fig. 11 the differences in SMB between 2100/2300 and 2000 as multi-year mean over five years each. The difference in SMB 2100-2000 of HadGEM2-ES indicates a similar pattern presented by Krapp et al. (2017) using MAR (Fettweis et al., 2013). Increasing SMB in the eastern part of the ice sheet with a maximum in the southern half of the ice sheet; at the ice sheet margins ablation is increased. The same pattern is characteristic for 2300-2000, but with a further increase of melting and decrease of accumulation in the center of the ice sheet. The SMB is reduced in the center, leaving a wide area with differences in SMB of $0.5\,\mathrm{m\,a^{-1}}$ and more, except for the ablation at the ice sheet margin. Moreover, most evident is a decreasing SMB in the Northeast. The SMB difference of IPSL-CM5A-LR is showing a similar pattern with enhanced amplitudes compared to HadGEM2-ES, in particular, an the southwestern margin; melting in the Southwest is increased up to $1\,\mathrm{m\,a^{-1}}$. In contrast a SMB gain is concentrated in the center-East and Northwest by 2300; the margin in the northwest is experiencing a SMB increase of $+1\,\mathrm{m\,a^{-1}}$. The most astonishing result is the ΔSMB pattern in MIROC5. Increasing SMB along the southwestern and southern margins in contrast to gently decreasing SMB in the center of the ice sheet. By 2300 ΔSMB the pattern changes and SMB is generally increasing in the East and decreasing at the western margins; the magnitude of ΔSMB is less compared to HadGEM2-ES and IPSL-CM5A-LR.

3.4 Ice thickness change and dynamic response

Extensive marginal thinning is experienced by forcing the ice sheet with HadGEM2-ES and IPSL-CM5A-LR (Fig. 13). In contrast to the mass loss near the margin the interior shows increased thickening; IPSL-CM5A-LR reveals more thickening in the interior. Generally the pattern correlates with observations (Helm et al., 2014) except that Petermann and Kangerdlusuaq glaciers shows an opposite trend. With a forcing of MIROC5 the pattern of the elevation change is different with thinning in the southern center of the ice sheet; the northern center experienced thickening. Although thinning occurs at the margin it is less extensive compared to the other GCMs. The ice tongue 79°N Glacier is in all forcings threatened in their existence, even with the moderate forcing of MIROC5.

The response of ice velocities to RCP2.6 forcing is presented in Fig. 14, where the change in horizontal surface velocities is shown for all scenarios as a difference between 2100–2000 and 2300–2000 (each as five year mean). For all GCM forcings the ice response shows relatively the same behaviour. The NEGIS, Jakobshavn Isbræ, Helheim, Ryder glaciers and Hagen Bræ experience acceleration; deceleration is present at Petermann and Kangerdlusuaq glaciers. However, the magnitude of response is among all models different. Most prominent at the western margin where HadGEM2-ES lead the strongest acceleration while MIROC5 to the lowest. Though, the acceleration of Jakobshavn Isbræ is present in our simulations, however, not to the extent of the observations (Joughin et al., 2014). This is due to the lack of forcing with calving rates in our simulations, which has been key for reproducing the observed acceleration and retreat in Bondzio et al. (2017).

4 Discussion

Fürst et al. (2015) performed a comprehensive ensemble study for a suite of 10 GCMs (HadGEM2-ES, IPSL-CM5A-LR and MIROC5 included) and four different RCP scenarios. For the RCP2.6 scenario they estimate an abated sea level contribution of 42.3±18.0 mm by 2100 and 88.2±44.8 mm by 2300. Our averaged result of a sea level contribution under RCP2.6 forcing is slightly lower but still in their ensemble variability. The resultant projection by Fürst et al. (2015) included contributions from lubrication, marine melt and SMB-coupling while ours account for SMB forcing only. The lubrication effect was diagnosed to have a negligible effect on the overall mass budget, but the oceanic influence on the total ice loss explains about half of the mass loss for RCP2.6. Since a future ocean forcing and calving front retreat is not considered here, the response of the ice sheet is likely underestimated here. By 2010 the cumulative ice discharge for HadGEM2-ES contributes with about 15% to the ice loss. By 2100 and 2300 the contribution is below 3 and 7%, respectively and becomes negligible. For IPSL-CM5A-LR and MIROC5 the cumulative effect of ice discharge shares less than 10% of the total mass budget by 2010 and 2100 but increases towards 17% by 2300. The different behaviour can be explained by the interaction with the SMB and ice dynamics as the relative importance of outlet glacier dynamics decreases with increasing surface melt (Goelzer et al., 2013; Fürst et al., 2015). Increased ice discharge causes dynamic thinning further upstream, lowering of the ice surface and thereby intensifies surface melting due to the associated warming of the near surface. Surface melting in turn competes with the discharge increase by removing ice before it reaches the marine margin. The simulated increase of ice discharge for IPSL-CM5A-LR and MIROC5 is therefore linked to the recovery of SMB of the course of the 22^{nd} century. Still, the SMB remains the dominant factor for mass loss. The speed-up observed from all scenarios merely transport ice form the interior but is melted before it reaches the ice sheet margin. However, the values for sea level contribution of this study may serve as a lower bound, as processes proven to play a major role in GrIS mass loss are not yet represented by the model.

Additionally, the calculation of the surface mass balance are based on different methods. Fürst et al. (2015) rely on the rather simple and empirical derived PDD scheme, while we use an more advanced energy-balance approach. So far the sensitivity of melting to warming of these class of models is not well understood. Comparisons of PDD models and energy-balance models suggested that the former are too sensitive to climate change and produce a larger runoff response (van de Wal, 1996; Bougamont et al., 2007; Graversen et al., 2011). On the other hand Goelzer et al. (2013) attempted to make a robust comparison and find that a PDD model underestimates sea level rise by 14–31% compared to MAR. An Assessment of the SMB and its impact on sea level contribution calculated by the PDD scheme in Fürst et al. (2015) and the SEMIC model from this study cannot be drawn, because of the strong interaction between ice loss, ice dynamics and external forcings. As the cumulative discharge rates in the mass budget are higher compared to Fürst et al. (2015) may indicate a lower SMB forcing. However, compared to other models that participate in the initMIP-GrIS exercise (Goelzer et al., 2018), our setup is whether on the higher end nor of the lower spectrum of estimated mass loss. Additionally, we have conducted SeaRISE experiments similar to Bindschadler et al. (2013), which showed us that we are within the spread among the models, in particular, for the amplified climatic scenarios C1, C2, and C3 (not shown here).

The modified RCP2.6 scenario without overshoot projected a sea level contribution that is on average about 38% and 31% less by 2100 and by 2300, respectively. For HadGEM2-ES and MIROC5 the partition of the mass budget is relatively similar to the scenario with overshoot but with a slightly increased cumulative discharge. For IPSL-CM5A-LR the behaviour is more irregular. It gains mass during the last century, as a result from an increasing SMB which is partly compensated by enhanced ice discharge up to 40%. However, the spread of sea level contribution is much larger compared to the RCP2.6 scenario with overshoot. In particular, in 2300 the range of sea level contribution is between 3.4–66.9 mm. The very low estimated contribution of 3.4 mm is a result from the IPSL-CM5A-LR forcing that predicts a relatively high SMB for the characteristic time of overshooting 1.5°C (Tab. 2). The SMB is close to present-day and therefore IPSL-CM5A-LR maintains a geometry close to present day. The prolongation of these scenarios were done by repeating the forcing from a time window that reveals a stabilized climate. Repeating the last 30-year forcing field window before the characteristic time is not reasonable, because the change in warming is strongest during that period and a stabilized climate would not be reached. In fact, we would generate a non-mitigation pathway scenario with constant warming rates that will have larger melt and therefore likely contributes more to sea level contribution (not shown here).

The generally abated sea level contribution confirms with the inferred threshold in global mean temperature before irreversible ice sheet topography changes occur. The simplified assumption behind these threshold is an integrated SMB over the whole ice sheet that becomes negative (Gregory and Huybrechts, 2006). Fettweis et al. (2013) reported a threshold of 3.5°C relative to pre-industrial, which is never exceeded under the RCP2.6 scenario. Assuming a steady state ice-sheet SMB of 400 Gt yr^{-1} the decline in SMB must be larger than -400 Gt yr^{-1} to get a continuous retreating ice sheet margin. If the mean SMB of the GrIS remains positive a new steady state ice sheet geometry may be possible, but require a balancing with the ice outflow.

At last we want to discuss if studying RCP2.6 allows to draw significant conclusions on the development of sea level rise due to mass loss in Greenland. We found that only a fraction of the current observed mass loss in the first two decades is represented by the model in RCP2.6. This can be attributed to different factors: the current emissions are above the RCP2.6 limit and hence the natural system evolves on a different route than RCP2.6. Secondly, the three GCMs are quite different in response to the RCP2.6 forcing and last but not least, the model itself does not represent all mechanisms, in particular the lack of oceanic forcing is causing a reduced sea level rise. Hence, a new emission scenario, that represent the real RCP pathway in the recent past, would be most useful for future studies like ours.

5 Conclusions

We have applied climate forcings based on the low-emission scenario CMIP5 RCP2.6 of three underlying GCMs (HadGEM2-ES, IPSL-CM5A-LR, MIROC5) to ISSM. Despite all three GCMs are based on RCP2.6, their temperature variation – globally and regionally for GrIS – is considerably large. Arctic amplification causes a near-surface air temperature increase over Greenland by a factor of $\approx$ 2.4 and 2 in HadGEM2-ES and IPSL-CM5A-LR, respectively. MIROC5 reveals nearly no arctic amplification. In order to force the ice sheet model with a reliable SMB, a physically based surface energy balance model was applied. The estimated sea level contribution for the RCP2.6 peak and decline scenario is ranging in our simulations from 21–38 mm by 2100 and 36–85 mm by 2300 and are up to 30–40% higher compared to a scenario without overshoot. Despite the reduced SMB is the warmer climate, a future steady-state ice sheet with lower surface and volume might be possible.

Although the thickness change pattern agrees well with observations and acceleration of NEGIS, Helheim Glacier and Jakobshavn Isbræ is captured in our simulations, the estimated sea level contribution is potentially underestimated due to the following drawbacks of our study: (i) retreat of glaciers due to oceanic forcing (melt at vertical cliffs and/or calving rates) and (ii) seasonality due to lubrication arising from supra-glacial melt water is not included. This leads to the conclusion that the projections may serve as a lower bound of the contribution of Greenland to sea level rise under RCP2.6 climate scenario. This limits also the advantageous treatment of the physics in our model setup, meaning that all the benefits from a high-resolution higher order model are not yet contributing to the extent they potentially could. Our results further indicate, that uncertainties stem from the underlying climate model to calculate the surface mass balance.

Code availability. The ice sheet model ISSM is available at issm.jpl.nasa.gov and not distributed by the authors of this manuscript. SEMIC is available from https://gitlab.pik-potsdam.de/krapp/semic-project and not distributed by the authors of this manuscript.

Author contributions. M.R. conducted ISSM simulations, coupled SEMIC output to ISSM. M.R. and A.H. designed the study, analysed the results and wrote major parts of the manuscript. K.F. and S.L. selected, prepared and contributed GCM forcings. U.F. has contributed advice on the albedo scheme and checked the GCM input data.

Competing interests. There are no competing interests present.

Acknowledgements. This work was funded by BMBF under grant EP-GrIS (01LS1603A) and the Helmholtz Alliance Climate Initiative (REKLIM). We would like to thank both reviewers for the detailed review containing many helpful remarks and constructive criticism that helps to improve the manuscript. We acknowledge the technical support given by Mario Krapp (PIK) with SEMIC. We are grateful for the NetCDF interface to SEMIC provided by Paul Gierz (AWI). We would like to thank Vadym Aizinger, Natalja Rakowsky and Malte Thoma for maintaining excellent computing facilities at AWI. We also enthusiastically acknowledge the general support of the ISSM team.

References

Aschwanden, A., Bueler, E., Khroulev, C., and Blatter, H.: An enthalpy formulation for glaciers and ice sheets, Journal of Glaciology, 58, 441–457, https://doi.org/10.3189/2012JoG11J088, 2012.

Bauer, E. and Ganopolski, A.: Comparison of surface mass balance of ice sheets simulated by positive-degree-day method and energy balance approach, Climate of the Past, 13, 819, 2017.

Beckmann, A. and Goosse, H.: A parameterization of ice shelf–ocean interaction for climate models, Ocean Modelling, 5, 157–170, https://doi.org/10.1016/S1463-5003(02)00019-7, 2003.

Bindschadler, R. A., Nowicki, S., Abe-Ouchi, A., Aschwanden, A., Choi, H., Fastook, J., Granzow, G., Greve, R., Gutowski, G., Herzfeld, U., Jackson, C., Johnson, J., Khroulev, C., Levermann, A., Lipscomb, W. H., Martin, M. A., Morlighem, M., Parizek, B. R., Pollard, D., Price, S. F., Ren, D., Saito, F., Sato, T., Seddik, H., Seroussi, H., Takahashi, K., Walker, R., and Wang, W. L.: Ice-sheet model sensitivities to environmental forcing and their use in projecting future sea level (the SeaRISE project), Journal of Glaciology, 59, 195–224, https://doi.org/doi:10.3189/2013JoG12J125, 2013.

Blatter, H.: Velocity and stress fields in grounded glaciers: a simple algorithm for including deviatoric stress gradients, Journal of Glaciology, 41, 333–344, 1995.

Bondzio, J. H., Seroussi, H., Morlighem, M., Kleiner, T., Rückamp, M., Humbert, A., and Larour, E. Y.: Modelling calving front dynamics using a level-set method: application to Jakobshavn Isbræ, West Greenland, The Cryosphere, 10, 497–510, https://doi.org/10.5194/tc-10-497-2016, 2016.

Bondzio, J. H., Morlighem, M., Seroussi, H., Kleiner, T., Rückamp, M., Mouginot, J., Moon, T., Larour, E. Y., and Humbert, A.: The mechanisms behind Jakobshavn Isbræ's acceleration and mass loss: A 3-D thermomechanical model study, Geophysical Research Letters, 44, 6252–6260, https://doi.org/10.1002/2017GL073309, 2017GL073309, 2017.

Bougamont, M., Bamber, J. L., Ridley, J. K., Gladstone, R. M., Greuell, W., Hanna, E., Payne, A. J., and Rutt, I.: Impact of model physics on estimating the surface mass balance of the Greenland ice sheet, Geophysical Research Letters, 34, https://doi.org/10.1029/2007GL030700, 2007.

Choi, Y., Morlighem, M., Rignot, E., Mouginot, J., and Wood, M.: Modeling the Response of Nioghalvfjerdsfjorden and Zachariae Isstrøm Glaciers, Greenland, to Ocean Forcing Over the Next Century, Geophysical Research Letters, 44, 11,071–11,079, https://doi.org/10.1002/2017GL075174.

Courant, R., Friedrichs, K., and Lewy, H.: Über die Partiellen Differenzengleichungen der Mathematischen Physik, Mathematische Annalen, 100, 32–74, 1928.

Dansgaard, W., Johnsen, S., Clausen, H., Dahl-Jensen, D., Gundestrup, N., Hammer, C., Hvidberg, C., Steffensen, J., Sveinbjörndottir, A., Jouzel, J., and Bond, G.: Evidence for general instability of past climate from a 250-kyr ice-core record, Nature, 364, 218–220, https://doi.org/doi:10.1038/364218a0, 1993.

Edwards, T. L., Fettweis, X., Gagliardini, O., Gillet-Chaulet, F., Goelzer, H., Gregory, J. M., Hoffman, M., Huybrechts, P., Payne, A. J., Perego, M., Price, S., Quiquet, A., and Ritz, C.: Probabilistic parameterisation of the surface mass balance elevation feedback in regional climate model simulations of the Greenland ice sheet, The Cryosphere, 8, 181–194, https://doi.org/10.5194/tc-8-181-2014, 2014a.

Edwards, T. L., Fettweis, X., Gagliardini, O., Gillet-Chaulet, F., Goelzer, H., Gregory, J. M., Hoffman, M., Huybrechts, P., Payne, A. J., Perego, M., Price, S., Quiquet, A., and Ritz, C.: Effect of uncertainty in surface mass balance elevation feedback on projections of the future sea level contribution of the Greenland ice sheet, The Cryosphere, 8, 195–208, https://doi.org/10.5194/tc-8-195-2014, 2014b.

Erokhina, O., Rogozhina, I., Prange, M., Bakker, P., Bernales, J., Paul, A., and Schulz, M.: Dependence of slope lapse rate over the Greenland ice sheet on background climate, Journal of Glaciology, 63, 568, https://doi.org/10.1017/jog.2017.10, 2017.

Ettema, J., van den Broeke, M. R., van Meijgaard, E., van de Berg, W. J., Bamber, J. L., Box, J. E., and Bales, R. C.: Higher surface mass balance of the Greenland ice sheet revealed by high-resolution climate modeling, Geophysical Research Letters, 36, n/a–n/a, https://doi.org/10.1029/2009GL038110, l12501, 2009.

Fettweis, X., Franco, B., Tedesco, M., van Angelen, J. H., Lenaerts, J. T. M., van den Broeke, M. R., and Gallée, H.: Estimating the Greenland ice sheet surface mass balance contribution to future sea level rise using the regional atmospheric climate model MAR, The Cryosphere, 7, 469–489, https://doi.org/10.5194/tc-7-469-2013, 2013.

Fettweis, X., Box, J. E., Agosta, C., Amory, C., Kittel, C., Lang, C., van As, D., Machguth, H., and Gallée, H.: Reconstructions of the 1900–2015 Greenland ice sheet surface mass balance using the regional climate MAR model, The Cryosphere, 11, 1015–1033, https://doi.org/10.5194/tc-11-1015-2017, https://www.the-cryosphere.net/11/1015/2017/, 2017.

Frieler, K., Lange, S., Piontek, F., Reyer, C. P. O., Schewe, J., Warszawski, L., Zhao, F., Chini, L., Denvil, S., Emanuel, K., Geiger, T., Halladay, K., Hurtt, G., Mengel, M., Murakami, D., Ostberg, S., Popp, A., Riva, R., Stevanovic, M., Suzuki, T., Volkholz, J., Burke, E., Ciais, P., Ebi, K., Eddy, T. D., Elliott, J., Galbraith, E., Gosling, S. N., Hattermann, F., Hickler, T., Hinkel, J., Hof, C., Huber, V., Jägermeyr, J., Krysanova, V., Marcé, R., Müller Schmied, H., Mouratiadou, I., Pierson, D., Tittensor, D. P., Vautard, R., van Vliet, M., Biber, M. F., Betts, R. A., Bodirsky, B. L., Deryng, D., Frolking, S., Jones, C. D., Lotze, H. K., Lotze-Campen, H., Sahajpal, R., Thonicke, K., Tian, H., and Yamagata, Y.: Assessing the impacts of 1.5 °C global warming – simulation protocol of the Inter-Sectoral Impact Model Intercomparison Project (ISIMIP2b), Geoscientific Model Development, 10, 4321–4345, https://doi.org/10.5194/gmd-10-4321-2017, https://www.geosci-model-dev.net/10/4321/2017/, 2017.

Fürst, J. J., Goelzer, H., and Huybrechts, P.: Ice-dynamic projections of the Greenland ice sheet in response to atmospheric and oceanic warming, The Cryosphere, 9, 1039–1062, https://doi.org/10.5194/tc-9-1039-2015, https://www.the-cryosphere.net/9/1039/2015/, 2015.

Gill, A. E.: Atmosphere-Ocean dynamics (International Geophysics Series), academic press, 1982.

GISTEMP Team: GISS Surface Temperature Analysis (GISTEMP), NASA Goddard Institute for Space Studies. Dataset accessed 2018-04-25 at https://data.giss.nasa.gov/gistemp/, 2018.

Goelzer, H., Huybrechts, P., Fürst, J., Nick, F., Andersen, M., Edwards, T., Fettweis, X., Payne, A., and Shannon, S.: Sensitivity of Greenland Ice Sheet Projections to Model Formulations, Journal of Glaciology, 59, 733–749, https://doi.org/10.3189/2013JoG12J182, 2013.

Goelzer, H., Nowicki, S., Edwards, T., Beckley, M., Abe-Ouchi, A., Aschwanden, A., Calov, R., Gagliardini, O., Gillet-Chaulet, F., Golledge, N. R., Gregory, J., Greve, R., Humbert, A., Huybrechts, P., Kennedy, J. H., Larour, E., Lipscomb, W. H., Le clec'h, S., Lee, V., Morlighem, M., Pattyn, F., Payne, A. J., Rodehacke, C., Rückamp, M., Saito, F., Schlegel, N., Seroussi, H., Shepherd, A., Sun, S., van de Wal, R., and Ziemen, F. A.: Design and results of the ice sheet model initialisation experiments initMIP-Greenland: an ISMIP6 intercomparison, The Cryosphere, 12, 1433–1460, https://doi.org/10.5194/tc-12-1433-2018, 2018.

Graversen, R. G., Drijfhout, S., Hazeleger, W., van de Wal, R., Bintanja, R., and Helsen, M.: Greenland's contribution to global sea-level rise by the end of the 21st century, Climate Dynamics, 37, 1427–1442, https://doi.org/10.1007/s00382-010-0918-8, 2011.

Gregory, J. and Huybrechts, P.: Ice-sheet contributions to future sea-level change, Philosophical Transactions of the Royal Society of London A: Mathematical, Physical and Engineering Sciences, 364, 1709–1732, https://doi.org/10.1098/rsta.2006.1796, http://rsta.royalsocietypublishing.org/content/364/1844/1709, 2006.

Greve, R.: Relation of measured basal temperatures and the spatial distribution of the geothermal heat flux for the Greenland ice sheet, Annals of Glaciology, 42, 424–432, 2005.

Helm, V., Humbert, A., and Miller, H.: Elevation and elevation change of Greenland and Antarctica derived from CryoSat-2, The Cryosphere, 8, 1539–1559, https://doi.org/10.5194/tc-8-1539-2014, 2014.

Huybrechts, P., Letreguilly, A., and Reeh, N.: The Greenland ice sheet and greenhouse warming, Palaeogeography, Palaeoclimatology, Palaeoecology, 89, 399 – 412, https://doi.org/https://doi.org/10.1016/0031-0182(91)90174-P, http://www.sciencedirect.com/science/article/pii/003101829190174P, 1991.

IPCC: Climate Change 2013: The Physical Science Basis. Contribution of Working Group I to the Fifth Assessment Report of the Intergovernmental Panel on Climate Change, Cambridge University Press, Cambridge, United Kingdom and New York, NY, USA, https://doi.org/10.1017/CBO9781107415324, www.climatechange2013.org, 2013.

Joughin, I., Smith, B. E., Shean, D. E., and Floricioiu, D.: Brief Communication: Further summer speedup of Jakobshavn Isbræ, The Cryosphere, 8, 209–214, https://doi.org/10.5194/tc-8-209-2014, https://www.the-cryosphere.net/8/209/2014/, 2014.

Kleiner, T., Rückamp, M., Bondzio, J. H., and Humbert, A.: Enthalpy benchmark experiments for numerical ice sheet models, The Cryosphere, 9, 217–228, https://doi.org/10.5194/tc-9-217-2015, 2015.

Krapp, M., Robinson, A., and Ganopolski, A.: SEMIC: an efficient surface energy and mass balance model applied to the Greenland ice sheet, The Cryosphere, 11, 1519–1535, https://doi.org/10.5194/tc-11-1519-2017, 2017.

Lange, S.: Bias correction of surface downwelling longwave and shortwave radiation for the EWEMBI dataset, Earth System Dynamics Discussions, 2017, 1–30, https://doi.org/10.5194/esd-2017-81, https://www.earth-syst-dynam-discuss.net/esd-2017-81/, 2017.

Larour, E., Seroussi, H., Morlighem, M., and Rignot, E.: Continental scale, high order, high spatial resolution, ice sheet modeling using the Ice Sheet System Model (ISSM), Journal of Geophysical Research: Earth Surface, 117, https://doi.org/10.1029/2011JF002140, 2012.

Meinshausen, M., Smith, S. J., Calvin, K., Daniel, J. S., Kainuma, M. L. T., Lamarque, J.-F., Matsumoto, K., Montzka, S. A., Raper, S. C. B., Riahi, K., Thomson, A., Velders, G. J. M., and van Vuuren, D. P.: The RCP greenhouse gas concentrations and their extensions from 1765 to 2300, Climatic Change, 109, 213, https://doi.org/10.1007/s10584-011-0156-z, https://doi.org/10.1007/s10584-011-0156-z, 2011.

Morlighem, M., Rignot, E., Seroussi, H., Larour, E., Dhia, H. B., and Aubry, D.: Spatial patterns of basal drag inferred using control methods from a full-Stokes and simpler models for Pine Island Glacier, West Antarctica, Geophysical Research Letters, 37, https://doi.org/10.1029/2010GL043853, https://agupubs.onlinelibrary.wiley.com/doi/abs/10.1029/2010GL043853, 2010.

Morlighem, M., Rignot, E., Mouginot, J., Seroussi, H., and Larour, E.: Deeply incised submarine glacial valleys beneath the Greenland ice sheet, Nature Geoscience, 7, 418–422, https://doi.org/10.1038/ngeo2167, 2014.

Morlighem, M., Bondzio, J., Seroussi, H., Rignot, E., Larour, E., Humbert, A., and Rebuffi, S.: Modeling of Store Gletscher's calving dynamics, West Greenland, in response to ocean thermal forcing, Geophysical Research Letters, 43, 2659–2666, https://doi.org/10.1002/2016GL067695, 2016GL067695, 2016.

Moss, R. H., Edmonds, J. A., Hibbard, K. A., Manning, M. R., Rose, S. K., van Vuuren, D. P., Carter, T. R., Emori, S., Kainuma, M., Kram, T., Meehl, G. A., Mitchell, J. F. B., Nakicenovic, N., Riahi, K., Smith, S. J., Stouffer, R. J., Thomson, A. M., Weyant, J. P., and Wilbanks, T. J.: The next generation of scenarios for climate change research and assessment, Nature, 463, 747–756, http://dx.doi.org/10.1038/nature08823, 2010.

Nerem, R. S., Beckley, B. D., Fasullo, J. T., Hamlington, B. D., Masters, D., and Mitchum, G. T.: Climate-change–driven accelerated sea-level rise detected in the altimeter era, Proceedings of the National Academy of Sciences, https://doi.org/10.1073/pnas.1717312115, http://www.pnas.org/content/early/2018/02/06/1717312115, 2018.

Noël, B., van de Berg, W., Lhermitte, S., Wouters, B., Machguth, H., Howat, I., Citterio, M., Moholdt, G., Lenaerts, J., and van den Broeke, M. R.: A tipping point in refreezing accelerates mass loss of Greenland's glaciers and ice caps, Nature Communications, 8, 14 730, 2017.

Noël, B., van de Berg, W. J., van Wessem, J. M., van Meijgaard, E., van As, D., Lenaerts, J. T. M., Lhermitte, S., Kuipers Munneke, P., Smeets, C. J. P. P., van Ulft, L. H., van de Wal, R. S. W., and van den Broeke, M. R.: Modelling the climate and surface mass balance of polar ice sheets using RACMO2 – Part 1: Greenland (1958–2016), The Cryosphere, 12, 811–831, https://doi.org/10.5194/tc-12-811-2018, https://www.the-cryosphere.net/12/811/2018/, 2018.

Nowicki, S., Bindschadler, R. A., Abe-Ouchi, A., Aschwanden, A., Bueler, E., Choi, H., Fastook, J., Granzow, G., Greve, R., Gutowski, G., Herzfeld, U., Jackson, C., Johnson, J., Khroulev, C., Larour, E., Levermann, A., Lipscomb, W. H., Martin, M. A., Morlighem, M., Parizek, B. R., Pollard, D., Price, S. F., Ren, D., Rignot, E., Saito, F., Sato, T., Seddik, H., Seroussi, H., Takahashi, K., Walker, R., and Wang, W. L.: Insights into spatial sensitivities of ice mass response to environmental change from the SeaRISE ice sheet modeling project II: Greenland, Journal of Geophysical Research: Earth Surface, 118, 1025–1044, https://doi.org/10.1002/jgrf.20076, 2013.

Nowicki, S. M. J., Payne, A., Larour, E., Seroussi, H., Goelzer, H., Lipscomb, W., Gregory, J., Abe-Ouchi, A., and Shepherd, A.: Ice Sheet Model Intercomparison Project (ISMIP6) contribution to CMIP6, Geoscientific Model Development, 9, 4521–4545, https://doi.org/10.5194/gmd-9-4521-2016, 2016.

Oerlemans, J. and Knap, W. H.: A 1 year record of global radiation and albedo in the ablation zone of Morteratschgletscher, Switzerland, Journal of Glaciology, 44, 231–238, https://doi.org/10.3189/S0022143000002574, 1998.

Pattyn, F.: A new three-dimensional higher-order thermomechanical ice sheet model: Basic sensitivity, ice stream development, and ice flow across subglacial lakes, Journal of Geophysical Research: Solid Earth, 108, https://doi.org/10.1029/2002JB002329, https://agupubs.onlinelibrary.wiley.com/doi/abs/10.1029/2002JB002329, 2003.

Pithan, F. and Mauritsen, T.: Arctic amplification dominated by temperature feedbacks in contemporary climate models, Nature Geoscience, 7, 181–184, https://doi.org/10.1038/ngeo2071, https://www.nature.com/articles/ngeo2071, 2014.

Price, S. F., Payne, A. J., Howat, I. M., and Smith, B. E.: Committed sea-level rise for the next century from Greenland ice sheet dynamics during the past decade, Proceedings of the National Academy of Sciences, 108, 8978–8983, https://doi.org/10.1073/pnas.1017313108, 2011.

Rietbroek, R., Brunnabend, S.-E., Kusche, J., Schröter, J., and Dahle, C.: Revisiting the contemporary sea-level budget on global and regional scales, Proceedings of the National Academy of Sciences, 113, 1504–1509, https://doi.org/10.1073/pnas.1519132113, 2016.

Rignot, E. and Mouginot, J.: Ice flow in Greenland for the International Polar Year 2008–2009, Geophysical Research Letters, 39, n/a–n/a, https://doi.org/10.1029/2012GL051634, 2012.

Rogelj, J., Luderer, G., Pietzcker, R. C., Kriegler, E., Schaeffer, M., Krey, V., and Riahi, K.: Energy system transformations for limiting end-of-century warming to below 1.5°C., Nature Clim. Change, 5, 519–527, http://dx.doi.org/10.1038/nclimate2572, 2015.

Seroussi, H., Morlighem, M., Rignot, E., Khazendar, A., Larour, E., and Mouginot, J.: Dependence of century-scale projections of the Greenland ice sheet on its thermal regime, Journal of Glaciology, 59, 1024–1034, https://doi.org/doi:10.3189/2013JoG13J054, 2013.

Seroussi, H., Morlighem, M., Larour, E., Rignot, E., and Khazendar, A.: Hydrostatic grounding line parameterization in ice sheet models, The Cryosphere, 8, 2075–2087, https://doi.org/10.5194/tc-8-2075-2014, 2014.

Shapiro, N. and Ritzwoller, M.: Inferring surface heat flux distributions guided by a global seismic model: Particular application to Antarctica, Earth and Planetary Science Letters, 223, 213–224, https://doi.org/10.1016/j.epsl.2004.04.011, 2004.

UNFCCC: Adoption of the Paris Agreement, Decision 1/CP.21 of FCCC/CP/2015/10/Add.1, available at: http://unfccc.int/resource/docs/2015/cop21/eng/10a01.pdf (last access: April 2018), 2015.

van de Wal, R. S. W.: Mass-balance modelling of the Greenland ice sheet: a comparison of an energy-balance and a degree-day model, Annals of Glaciology, 23, 36–45, https://doi.org/10.3189/S0260305500013239, 1996.

van den Broeke, M. R., Enderlin, E. M., Howat, I. M., Kuipers Munneke, P., Noël, B. P. Y., van de Berg, W. J., van Meijgaard, E., and Wouters, B.: On the recent contribution of the Greenland ice sheet to sea level change, The Cryosphere, 10, 1933–1946, https://doi.org/10.5194/tc-10-1933-2016, 2016.

Vizcaíno, M., Mikolajewicz, U., Jungclaus, J., and Schurgers, G.: Climate modification by future ice sheet changes and consequences for ice sheet mass balance, Climate Dynamics, 34, 301–324, https://doi.org/10.1007/s00382-009-0591-y, 2010.

Watterson, I. G., Bathols, J., and Heady, C.: What Influences the Skill of Climate Models over the Continents?, Bulletin of the American Meteorological Society, 95, 689–700, https://doi.org/10.1175/BAMS-D-12-00136.1, 2014.

Wilson, N., Straneo, F., and Heimbach, P.: Submarine melt rates and mass balance for Greenland's remaining ice tongues, The Cryosphere Discussions, 2017, 1–17, https://doi.org/10.5194/tc-2017-99, 2017.

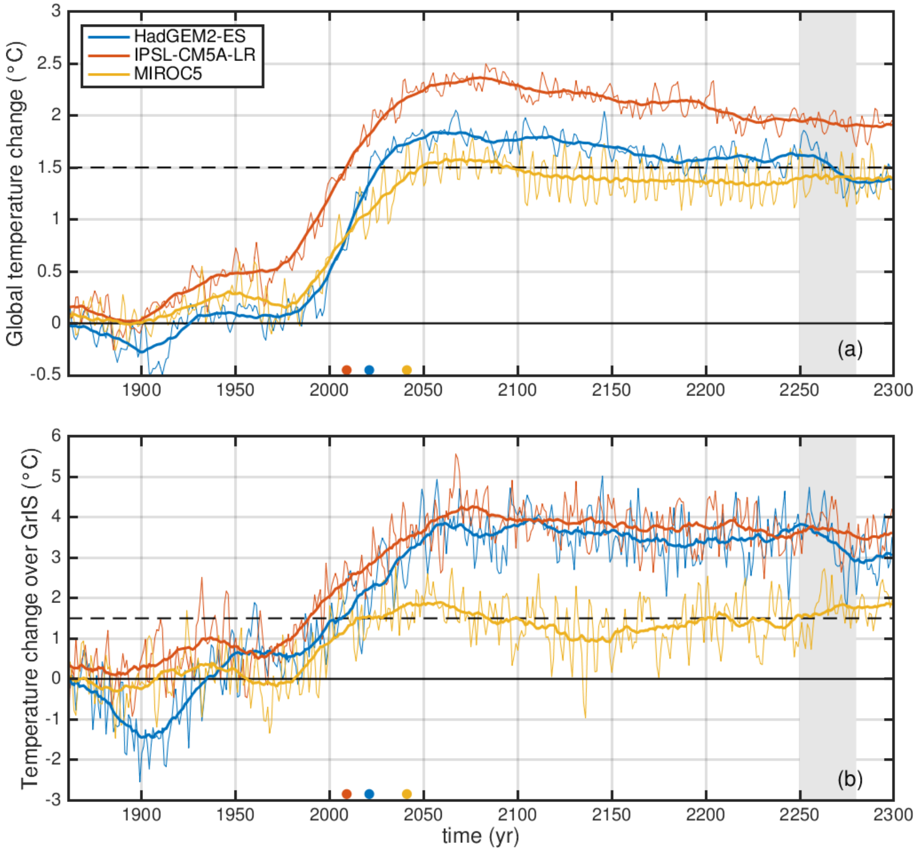

Figure 1. Time series of annual global mean near-surface temperature change (a) and over the GrIS (b) for all three GCMs relative to 1661–1880. The thick line is 30-year moving mean. The coloured dots represent the onset years of overshooting 1.5°C in the global mean near-surface air temperature in a 11-year moving window relative to pre-industrial levels. The light grey shaded area indicates the reused time period for the scenario without overshoot.

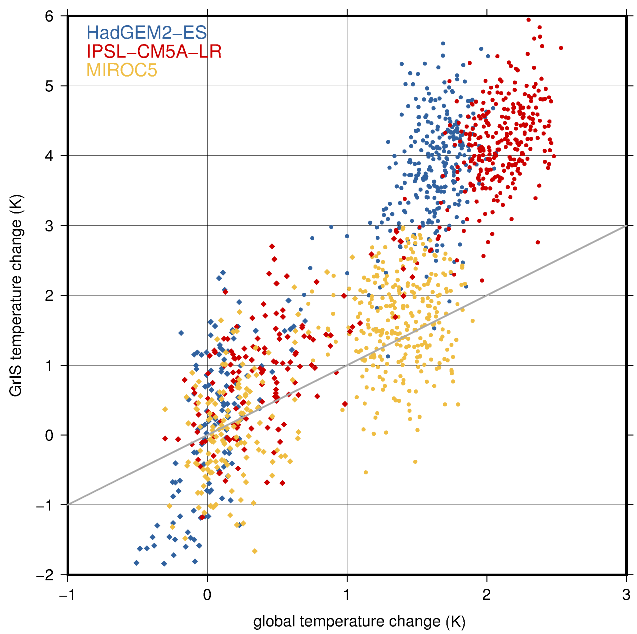

Figure 2. Scatter plot of annual mean near-surface air temperatures over GrIS versus annual global mean near-surface air temperatures for the years 1861–2299. The grey line depicts the identity.

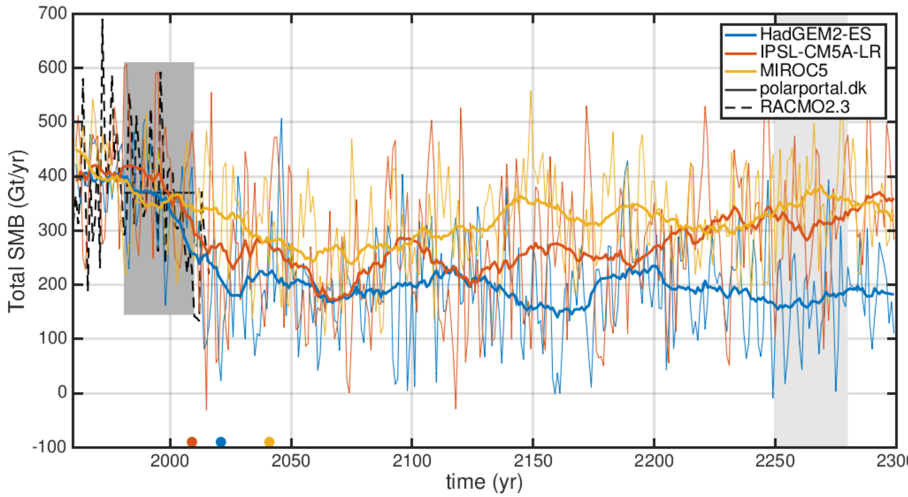

Figure 3. Time series of the annual mean integrated SMB_{clim} ($Gt\,yr^{-1}$) according to Eq. 3 for all three GCMs under RCP2.6 forcing. The thick line is a 30-year moving mean. In grey colour and black line the range and mean of SMB between 1981–2010 from Polarportal is marked (polarportal.dk). The dashed line shows the SMB time series of RACMO2.3 (Noël et al., 2018) from 1958-2016. The coloured dots represent the onset years of overshooting 1.5°C in the global mean near-surface air temperature in a 11 year moving window relative to pre-industrial levels. The light grey shaded area indicate the reused time period for the scenario without overshoot.

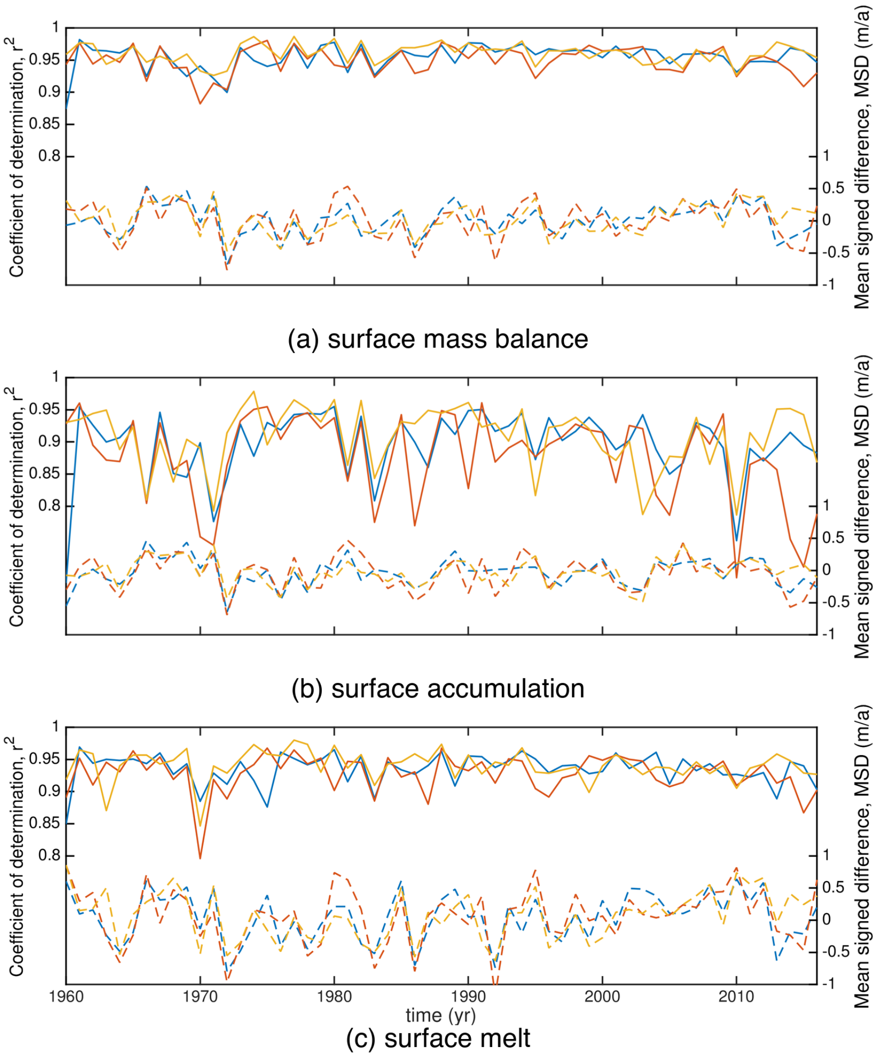

Figure 4. Coefficients of determination r^2 (straight lines and left y-axis) and mean singed difference MSD (dashed lines and right y-axis) between the GCM and RACMO2.3 SMB components. GCM colour code is the same as Fig. 3.

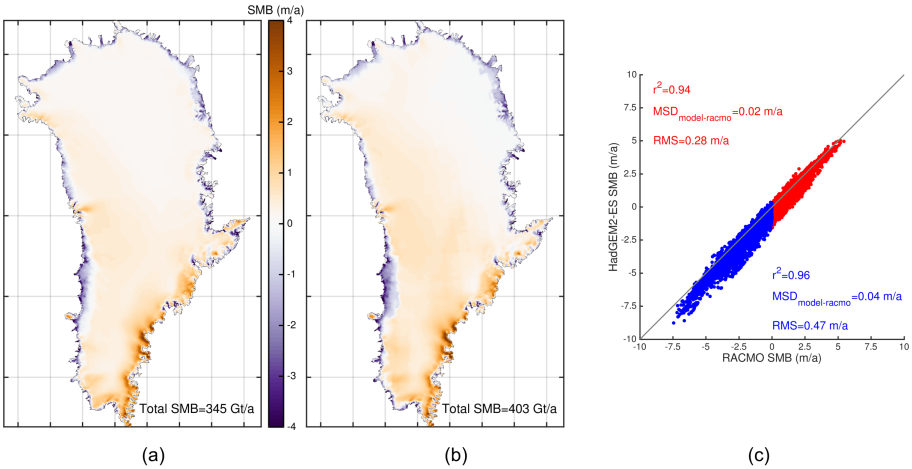

Figure 5. Comparison of the surface mass balance ($\mathrm{SMB}_{\mathrm{clim}}$) for the year 1990; (a) surface mass balance of RACMO2.3 (Noël et al., 2018); (b) surface mass balance for HadGEM2-ES according to Eq. 4; (c) scatter plot of both fields. Positive values represent accumulation (red dots); negative melting (blue dots) with respect to RACMO field.

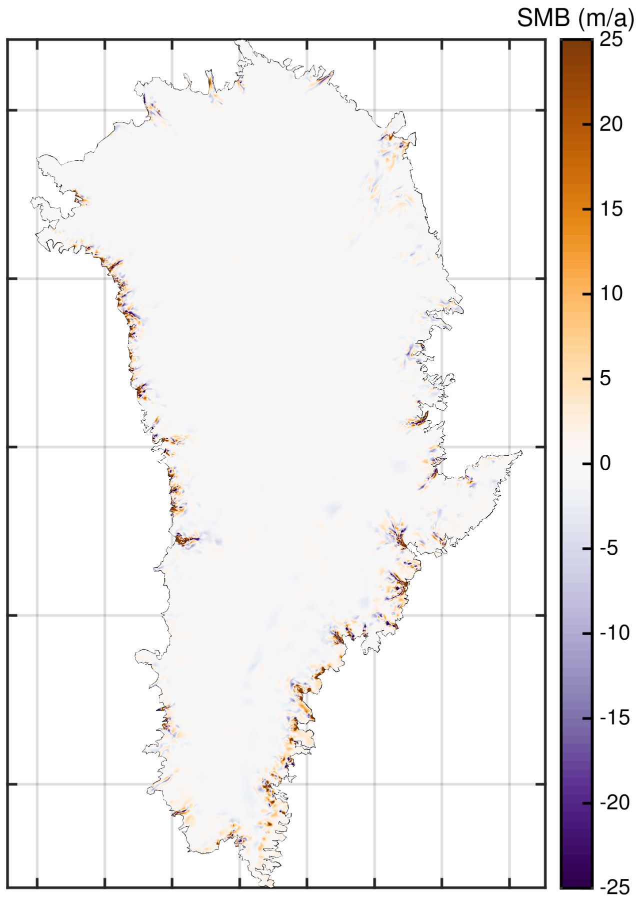

Figure 6. Synthetic surface mass balance $\mathrm{SMB_{corr}}$ calculated from an one year unforced relaxation run. As the $\mathrm{SMB_{corr}}$ will be subtracted in Eq. 8 positive values represent enforced thinning; negative values thickening.

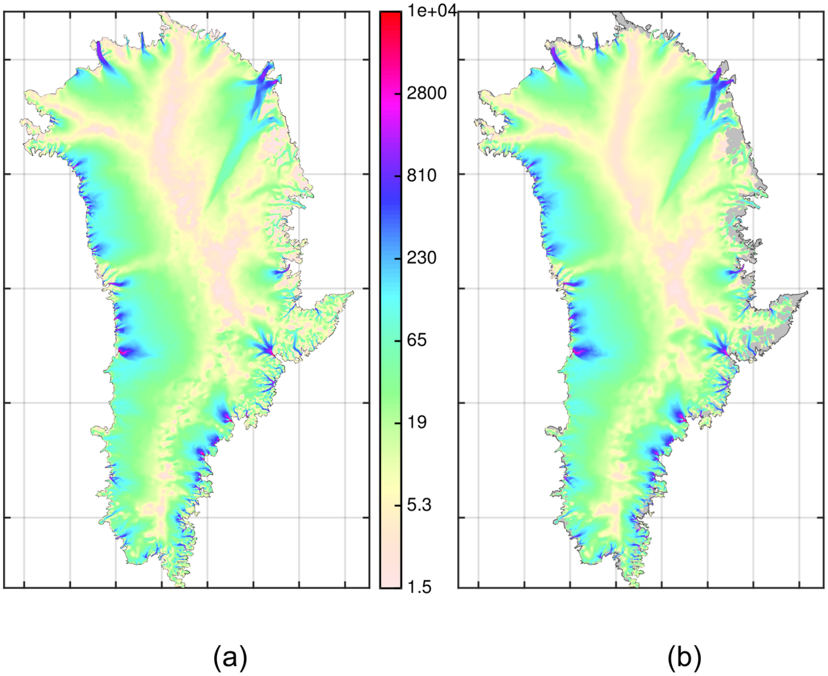

Figure 7. Present day velocities (year 2000) using HadGEM2-ES: (a) observed velocities, (b) simulated velocities. Observed velocities: Rignot and Mouginot (2012).

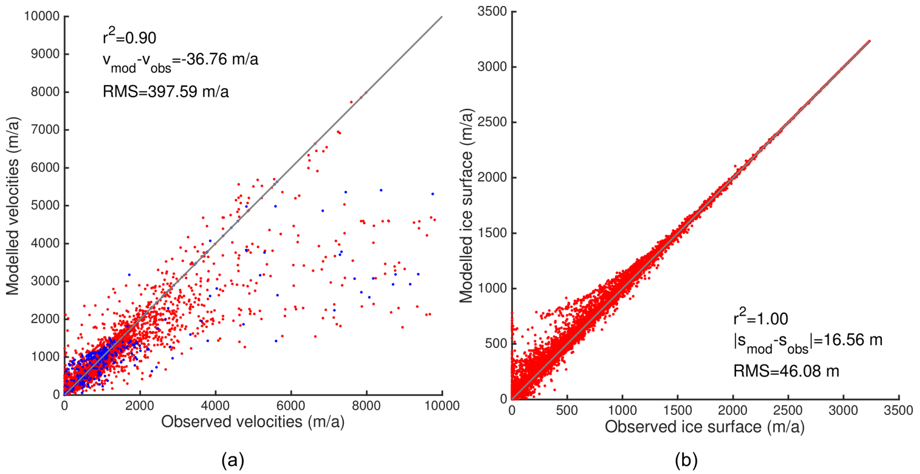

Figure 8. Scatter plots of the present day state (year 2000) using HadGEM2-ES: (a) velocities, (b) ice surface elevation. Observed velocities: Rignot and Mouginot (2012); Observed surface elevation: Morlighem et al. (2014).

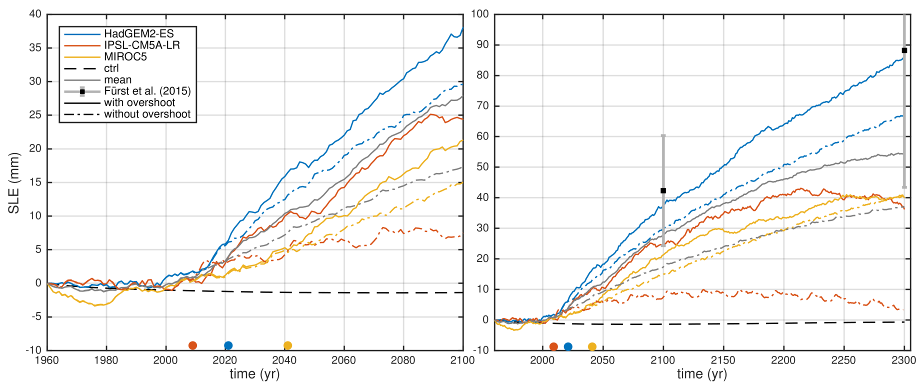

Figure 9. Sea level equivalent (SLE in mm) until the year 2100 (left panel) and 2300 (right panel) for all GCMs. Straight lines represent scenario with overshoot; dotted-dashed line without overshoot. Additionally the control run (black dashed line) and the model mean and rms deviation from Fürst et al. (2015, Table B1) are shown. The coloured dots represent the onset years of overshooting 1.5°C in the global mean near-surface air temperature in a 11-year moving window relative to pre-industrial levels.

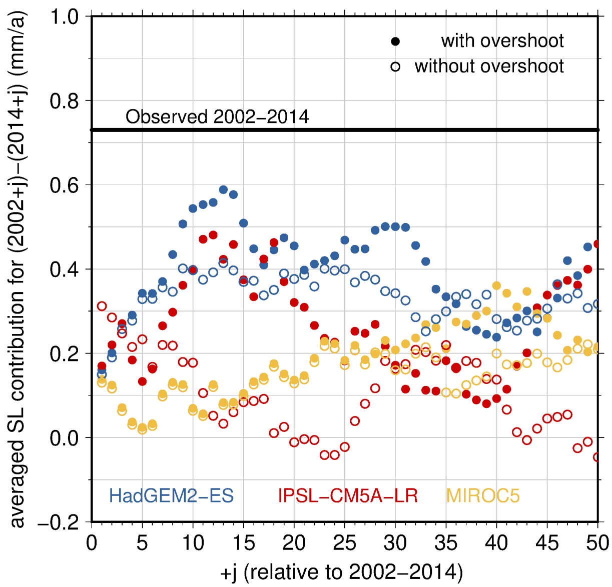

Figure 10. Lag (j) of projected sea level rise per year for three GCMs as mean for a time period similar to the observational period (2002–14). The black line indicates the observed value of 0.73 mm a^{-1} by Rietbroek et al. (2016).

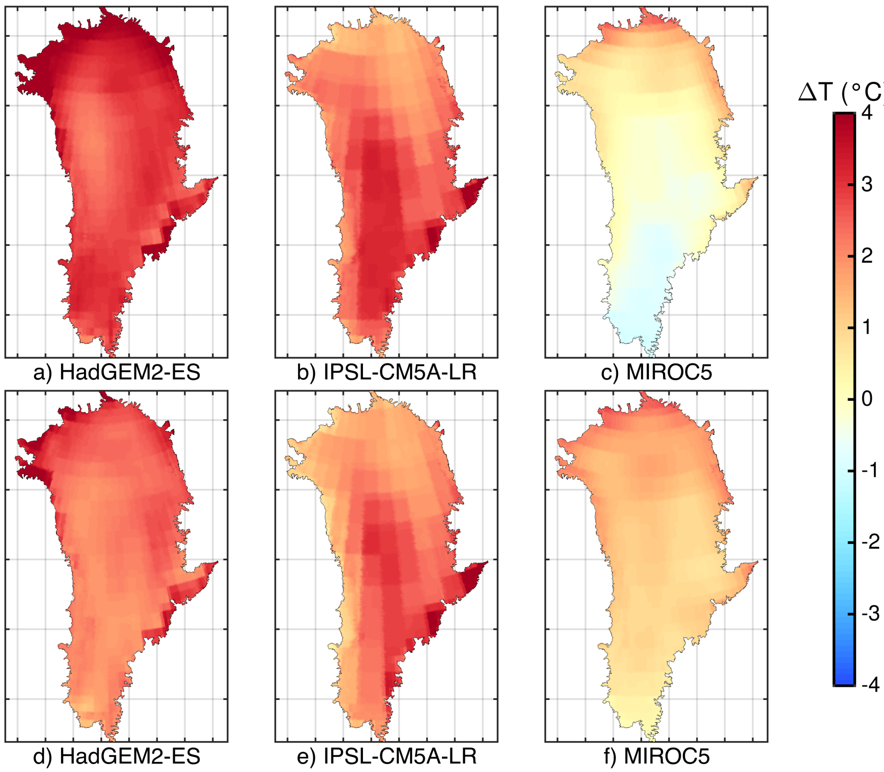

Figure 11. Comparison of multi-year mean surface temperature (T_s) differences between 2100-2000 (top row) and 2300-2000 (bottom row) for (a, d) HadGEM2-ES, (b, e) IPSL-CM5A-LR and (c, f) MIROC5. The black contour line depicts the present-day ice mask.

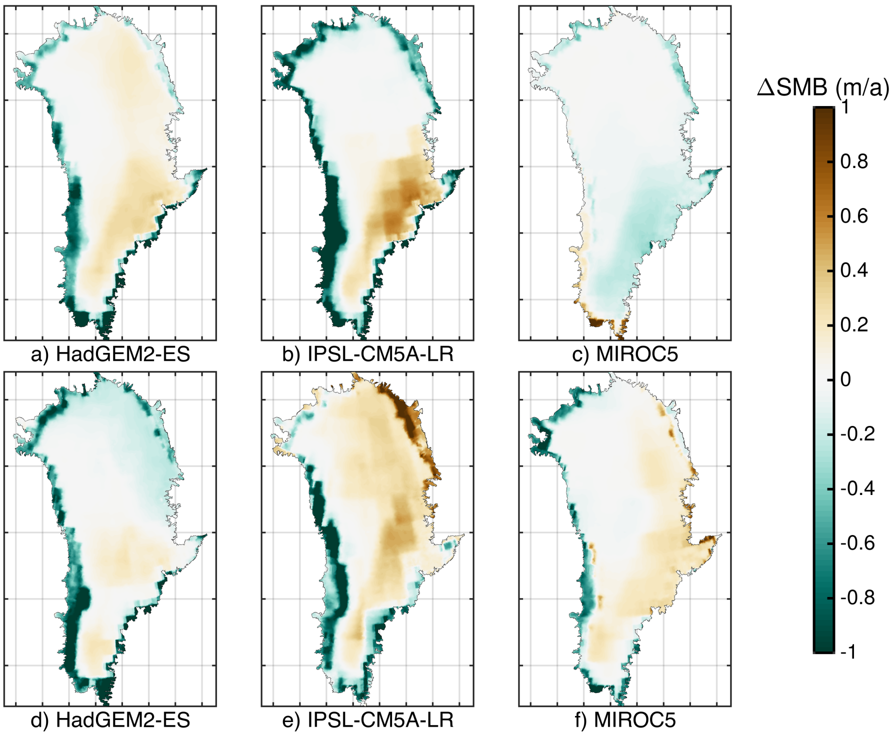

Figure 12. Comparison of multi-year mean surface mass balance (SMB) differences between 2100-2000 (top row) and 2300-2000 (bottom row) for (a, d) HadGEM2-ES, (b, e) IPSL-CM5A-LR and (c, f) MIROC5. The black contour line depicts the present-day ice mask.

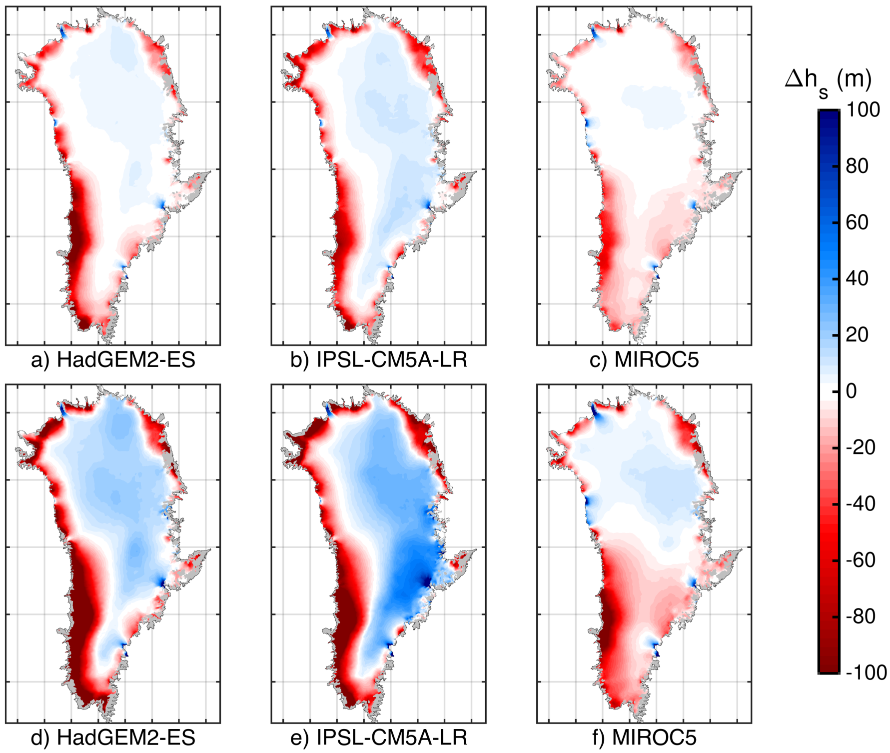

Figure 13. Comparison of multi-year mean surface elevation (h_s) differences between 2100-2000 (top row) and 2300-2000 (bottom row) for (a, d) HadGEM2-ES, (b, e) IPSL-CM5A-LR and (c, f) MIROC5. The black contour line depicts the present-day ice mask. Positive values represent glacier thinning; negative values thickenning. The data are clipped at ice thickness of 10 m (grey shaded area).

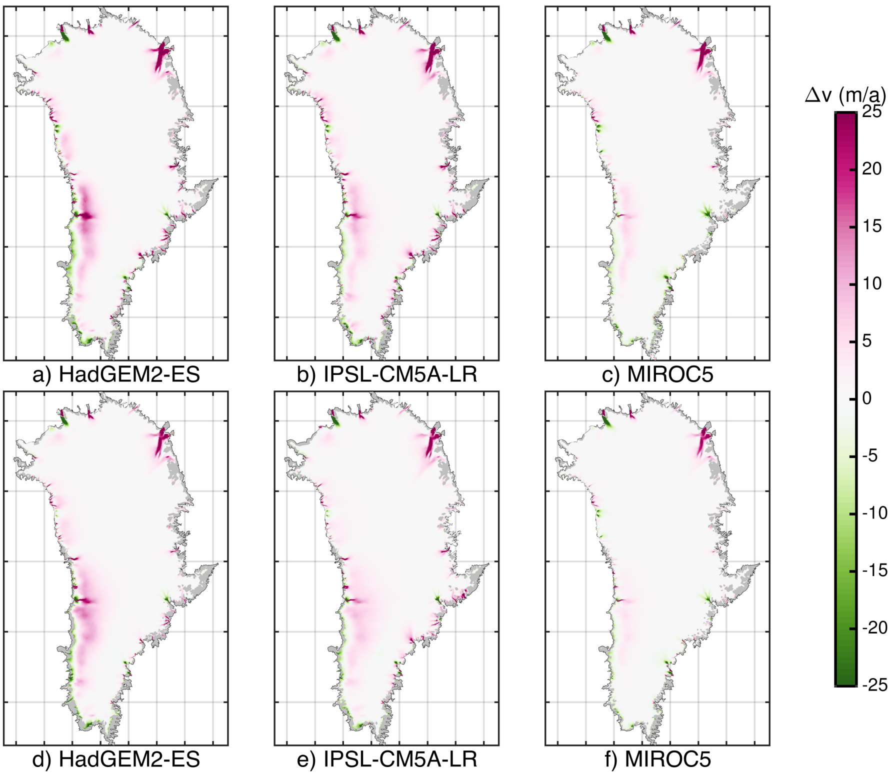

Figure 14. Comparison of multi-year mean surface velocity (v) differences between 2100-2000 (top row) and 2300-2000 (bottom row) for (a, d) HadGEM2-ES, (b, e) IPSL-CM5A-LR and (c, f) MIROC5. The black contour line depicts the present-day ice mask. Positive values represent glacier acceleration; negative values deceleration. The data are clipped at ice thickness of 10 m (grey shaded area).